







RESEARCH ARTICLE

WILEY

Diurnal cycle of surface energy fluxes in high mountain terrain: High-resolution fully coupled atmosphere-hydrology modelling and impact of lateral flow

Zhenyu Zhang^{1,2}  | Joël Arnault¹  | Patrick Laux^{1,2}  | Ning Ma³  | Jianhui Wei¹  | Harald Kunstmann^{1,2} 

¹Institute of Meteorology and Climate Research (IMK-IFU), Karlsruhe Institute of Technology, Campus Alpin, Garmisch-Partenkirchen, Germany

²Institute of Geography, University of Augsburg, Augsburg, Germany

³Key Laboratory of Water Cycle and Related Land Surface Processes, Institute of Geographic Sciences and Natural Resources Research, Chinese Academy of Sciences, Beijing, China

Correspondence

Zhenyu Zhang, Institute of Meteorology and Climate Research (IMK-IFU), Karlsruhe Institute of Technology, Campus Alpin, Garmisch-Partenkirchen, Germany.
Email: zhenyu.zhang@kit.edu

Funding information

German Federal Ministry of Science and Education (Bundesministerium für Bildung und Forschung), Grant/Award Number: 01LL1701B; China Scholarship Council; Deutsche Forschungsgemeinschaft, Grant/Award Numbers: AR 1183/2-1, KU 2090/11-1; National Natural Science Foundation of China, Grant/Award Number: 41801047

Abstract

Water and energy fluxes are inextricably interlinked within the interface of the land surface and the atmosphere. In the regional earth system models, the lower boundary parameterization of land surface neglects lateral hydrological processes, which may inadequately depict the surface water and energy fluxes variations, thus affecting the simulated atmospheric system through land-atmosphere feedbacks. Therefore, the main objective of this study is to evaluate the hydrologically enhanced regional climate modelling in order to represent the diurnal cycle of surface energy fluxes in high spatial and temporal resolution. In this study, the Weather Research and Forecasting model (WRF) and coupled WRF Hydrological modelling system (WRF-Hydro) are applied in a high alpine catchment in Northeastern Tibetan Plateau, the headwater area of the Heihe River. By evaluating and intercomparing model results by both models, the role of lateral flow processes on the surface energy fluxes dynamics is investigated. The model evaluations suggest that both WRF and coupled WRF-Hydro reasonably represent the diurnal variations of the near-surface meteorological fields, surface energy fluxes and hourly partitioning of available energy. By incorporating additional lateral flow processes, the coupled WRF-Hydro simulates higher surface soil moisture over the mountainous area, resulting in increased latent heat flux and decreased sensible heat flux of around 20–50 W/m² in their diurnal peak values during summertime, although the net radiation and ground heat fluxes remain almost unchanged. The simulation results show that the diurnal cycle of surface energy fluxes follows the local terrain and vegetation features. This highlights the importance of consideration of lateral flow processes over areas with heterogeneous terrain and land surfaces.

KEYWORDS

alpine area, complex terrain, diurnal cycle, feedback, fully coupled WRF-Hydro model, Heihe River, lateral flow, surface energy fluxes

This is an open access article under the terms of the Creative Commons Attribution-NonCommercial License, which permits use, distribution and reproduction in any medium, provided the original work is properly cited and is not used for commercial purposes.

© 2021 The Authors. *Hydrological Processes* published by John Wiley & Sons Ltd.

1 | INTRODUCTION

Water and energy fluxes are the key components of the land-atmosphere interface and play an important role in modulating weather and climate variability from local to global scale (Gentine et al., 2019; Suni et al., 2015). Understanding water and energy exchanges remains a challenge, as the landscape heterogeneity largely influences the interactions between the land surface and atmosphere dynamics in both spatial and temporal scales (Jimenez et al., 2014; Santanello et al., 2018). Investigating the land-atmosphere interactions over mountainous areas with complex orography often relied on point-scale measurements exclusively, thus showed limitations in the spatial coverage. Therefore, numerical simulations are widely used as a complement to observations for investigating the dynamics of land surface fluxes (Chakraborty et al., 2019; Erlandsen et al., 2017; Santanello et al., 2009; Xiang et al., 2017).

Several land surface models (LSMs) have been developed and strengthened in recent years for improving their performance in simulating surface energy and hydrologic components over mountainous areas (e.g., Chakraborty et al., 2019; Gao et al., 2015; Niu et al., 2011; Rosero et al., 2011; Xiang et al., 2017; Zheng et al., 2015). Coupled with LSMs, weather and climate models have shown their ability in reproducing interactions between soil, vegetation and the atmosphere (Aas et al., 2015; Erlandsen et al., 2017; Jousse et al., 2016; Sun et al., 2017), and have been used to investigate the impact of land surface conditions on the surface water and energy exchanges (Harding & Snyder, 2012; Yang et al., 2012). Nevertheless, these modelling approaches are afflicted by biases and uncertainties associated with model structures, parameter combinations, boundary conditions, and initial states (Chakraborty et al., 2019; Dumedah & Walker, 2014; Jousse et al., 2016; Orth et al., 2016). It has been pointed out that proper representing the hydrological processes in the land surface, for example, the lateral flow, can be of relevance to provide an improved understanding of land surface-atmosphere interactions (Davison et al., 2018; Fan et al., 2019; Maxwell et al., 2015; Senatore et al., 2015).

Novel fully coupled atmospheric-hydrological models have been developed to interlink the land surface hydrology within the weather and climate model framework (e.g., Davison et al., 2018; Gochis et al., 2015; Shrestha et al., 2014; Wagner et al., 2016). Accordingly, lateral flow in the terrestrial surface was found to have influences on the simulation of regional climate and water systems. For instance, Kerandi et al. (2018), Rummler et al. (2019), and Zhang et al. (2019) employed Weather Research and Forecasting model (WRF) and coupled WRF-Hydro for investigating the joint atmospheric-hydrological water balances over East Africa, Eastern Alps, and North-east fringe of Tibet Plateau, respectively. These studies indicated that the lateral hydrological processes altered the regional water cycle, thus affecting local precipitation recycling. Over a Mediterranean catchment in southern Italy, Senatore et al. (2015) found that the inclusion of the lateral flow slightly decreased the simulated precipitation during autumn and wintertime. Furthermore, Arnault et al. (2018, 2021) found that the resolved lateral flow increased the uncertainties

of modelled precipitation and enhanced the positive soil moisture-precipitation feedback over Europe and West Africa. Wehbe et al. (2019) employed coupled WRF-Hydro modelling in a hyper-arid environment over Arabian Peninsula, and their results showed that the precipitation and radiation forecasts were improved when the lateral surface flow was enrolled in the operational forecasting. Considering the groundwater lateral flow, Shrestha et al. (2014) carried out both idealized and real data simulations with Terrestrial Systems Modelling Platform (TerrSysMP) and found that groundwater lateral flow systematically modified the root zone soil moisture and energy fluxes distributions. By comparing two coupled modelling platforms ParFlow-WRF and TerrSysMP, Sulis et al. (2017) showed the differences of heat and moisture budget in the land surface and atmospheric boundary layer, revealing the sensitivities of diurnal atmospheric processes to the lateral groundwater flow parameterization. In the case of a headwater region in the Rocky Mountain, Forrester and Maxwell (2020) reported that lateral transport of groundwater modified the coupling strength between evaporative fraction and atmospheric boundary layer in the summertime.

The above case-studies demonstrate that including lateral flow processes with atmospheric models broadly affects the simulated terrestrial and atmosphere systems. Still, the influence of lateral flow on the land-atmosphere interface is largely dependent on the region's local features as well as on the temporal and spatial scales used for the analysis. Ji et al. (2017) suggested that topography-induced lateral flow transport caused wetter valleys and drier peaks, thus modifying the latent heat around 8% ~ 12%. Zhang et al. (2019) concluded that the soil moisture was increased over the root zone in mountainous areas, while not much affected over the flat and arid areas. Over the relatively flat southern Great Plains, Yang et al. (2021) found that the lateral flow generally increased soil moisture over the lower elevations, with a stronger signal over steeper terrain. Considering the land surface-atmosphere feedbacks at a diurnal scale, Fersch et al. (2020) and Lahmers et al. (2020) compared WRF and fully coupled WRF-Hydro simulations with extensive site observations over the pre-alpine region in southern Germany and the North American monsoon region, respectively. These authors found a considerable modelling bias in terms of near-surface water and energy conditions, and further showed the extent of the impact of lateral flow varying from site to site. Therefore, it is important to further investigate the utility of the current coupled modelling system as well as the impact of lateral flow, over regions characterized by diverse orography, climatic and hydrological conditions. Moreover, evaluating the diagnostic variables such as surface energy fluxes is relevant for characterizing surface feedbacks on the atmosphere.

The present study proceeds with the physically-improved realism of the fully coupled atmosphere-hydrological model by considering lateral flow redistribution in the terrestrial surface. The objectives of this study are:

1. To evaluate the performance of the fully coupled atmospheric-hydrological model for reproducing the diurnal surface meteorological fields and energy fluxes;

2. To investigate the impact of lateral flow on the simulated surface energy fluxes at a diurnal scale; and
3. To explore diurnal features of surface energy fluxes over the mountainous area with heterogeneous land surface.

For the investigation, the headwater area of Heihe River located at the Northeastern Tibetan Plateau is selected as a case study. The mid- and downstream areas of this river seriously suffer from water shortage, water supply and management, and ecosystem deterioration issues (Cheng et al., 2014). This headwater area is characterized by a sharp topography gradient and diversified landscape with very high elevation (1650 ~ 5500 m a.s.l.), and its hydrological and ecosystem conditions are sensitive to climate variability (Li et al., 2018; Zhang et al., 2016). Therefore, it is relevant to understand the role of lateral flow processes on water, energy and atmosphere interactions in this area. We carry out WRF and coupled WRF-Hydro modelling at the Heihe River basin from 2008 to 2010, and particularly focus on the simulation of the diurnal cycle of surface meteorological conditions and energy fluxes. The performance of simulations is assessed at point-scale using in-situ measurements and at basin-scale using gridded references. In addition, the impact of lateral flow is investigated by intercomparing the coupled WRF-Hydro with stand-alone WRF simulations. To our knowledge, this study represents the first effort to investigate the impact of lateral flow on diurnal surface energy fluxes over the alpine area.

In the following, the study area characteristics and observational data are briefly described in Sections 2.1 and 2.2, respectively. The

modelling strategy is described in Section 2.3 and the evaluation criteria are shown in Section 2.4. The validation of model simulations is presented in Section 3. Results from model evaluation and the impacts of coupled modelling are further discussed in Section 4, and conclusions are included in Section 5.

2 | MATERIALS AND METHODOLOGY

2.1 | Characteristics of study region

The study region, the Heihe River basin, is located in Northwestern China (Figure 1a). It is the second-largest endorheic river basin in China with an area around 143 000 km². The Heihe River stretches from the southern Qilian Mountains of the Tibetan Plateau to the northern high-plain area of the Gobi Desert, with elevations ranging from about 5500–1000 m. Exiting the mountains region, most of the rivers disappear at natural oases in the midstream, due to the high infiltration and irrigation usage (Chen et al., 2018). This study focuses on the headwater catchment of the Heihe River mainstream. This headwater area is defined as the drainage region at the Yingluoxia gauging station, encompassing an area of about 10 000 km² (Figure 1b), and it is away from human activities. The land cover is -elevation-dependent, with forest-steppe, alpine meadow and permanent cold zones from low valleys to high mountains crests, and the primary soil type is frigid desert soil (Zhang et al., 2016). This area is characterized by large seasonal temperature and precipitation

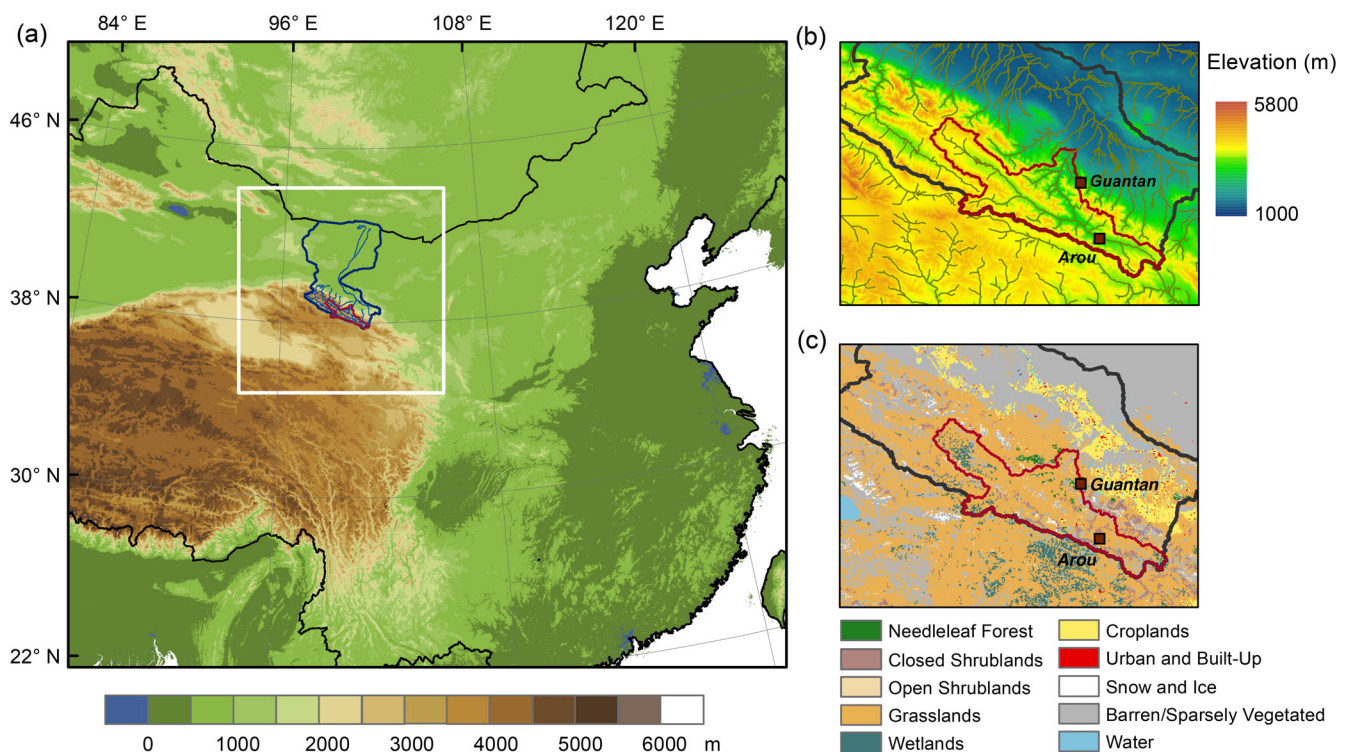


FIGURE 1 (a) The location of the Heihe River basin and the WRF/WRF-Hydro simulation domain. Zoom of the (b) topography and streams around the headwater of Heihe River, with the location of EC stations, and the (c) vegetation cover around the headwater area of Heihe River, derived from Multisource Integrated Chinese Land Cover Map from Ran et al. (2012)

variability. The mean annual temperature is ranging between -3 and $+3^{\circ}\text{C}$. The annual precipitation varies from 200 to 700 mm, increasing from west to east and increasing noticeably with elevation (Pan et al., 2012). Most precipitation occurs between May and September, accounting for more than 80% of the total annual amounts.

2.2 | Dataset

The simulated diurnal surface meteorological conditions are validated with the China Meteorological Forcing dataset (CMFD). The CMFD dataset provides the gridded surface meteorological elements at 3-hourly temporal and 0.1-degree spatial resolution. It is produced by merging records from more than 700 weather stations of China Meteorological Administration with various global background data sources (He et al., 2020). A wide range of validation studies (e.g., Pan et al., 2014; Yang et al., 2017) suggested that CMFD accurately represents the spatiotemporal variability of the meteorological condition. For this reason, CMFD has been widely used for not only driving the LSMs and hydrological models (e.g., Ma et al., 2019; Yuan et al., 2018), but also assessing the impact of climate change in China (e.g., Chu et al., 2015; Zhao et al., 2016).

Measurements at two ground-based alpine hydrometeorological observatory stations (Figure 1b), namely Arou station and Guantan station, established within the Heihe Watershed Allied Telemetry Experimental Research project (Li et al., 2013), are used for validating the simulated diurnal meteorological variables and energy fluxes. Both sites use the eddy covariance (EC) method to measure the sensible and latent heat fluxes near surface. The Arou station ($100^{\circ}27'\text{E}$, $38^{\circ}03'\text{N}$, and 3033 m a.s.l.) is established above a flat natural alpine meadow with the height of 2.8 m. The mean annual temperature at Arou station is -0.4°C , so that the feedbacks from the soil freeze-thaw process are monitored. The Guantan station ($100^{\circ}15'\text{E}$, $38^{\circ}32'\text{N}$, and 2835 m a.s.l.) is located in a forest ecosystem, with the height of 20.3 m above ground, underlying with overstory trees of Qinghai spruce (*Picea crassifolia*). The canopy height within its footprint area ranges from 15 to 20 m. The Guantan EC tower measures the energy components between the canopy and the atmosphere. Details on the site information and measurement instruments can be found in Liu et al. (2011) and Li et al. (2013). The raw 10 Hz data measured by the EC towers are processed into 30-min values with some partial gaps primarily due to weather and sensor failures. The data gaps are filled with the marginal distribution sampling method (Reichstein et al., 2005). The 30-min averaged fluxes values are further aggregated to hourly data for use in the model validations.

2.3 | WRF and WRF-Hydro modelling

In this study, we carry out two simulations: one with the stand-alone Advanced Research WRF version 3.7 (Skamarock et al., 2008) and another with the online coupled WRF-Hydro (Gochis et al., 2015). Both simulations have the same atmospheric domain setting, physical

parameterizations, lateral boundary forcing and initial conditions. The coupled WRF-Hydro model considers lateral flow processes in the land surface and permits the feedbacks from lateral flow to atmosphere. Both WRF and WRF-Hydro runs are performed for the period 2008–2010.

2.3.1 | WRF configuration

The atmospheric lateral boundary conditions are provided by operational analysis products from the European Center for Medium-Range Weather Forecast (ECMWF) with a resolution of 0.125° and 6 hourly temporal intervals. The initial conditions are provided by a 2-year WRF spin-up simulation to optimize an equilibrium state of soil moisture. Acknowledging a large impact of refined land surface static information on the simulated near-surface meteorological fields around the study area (Gao et al., 2008; Meng et al., 2009), we update the land cover map by the Multisource Integrated Chinese Land Cover Map (Ran et al., 2012) and the soil texture map by the Chinese 1:1 000 000 scale Soil Map from Harmonized World Soil Database, ensuring a comparable underlying condition between the EC sites and model grid points.

In the atmospheric setting, considering the convection-permitting modelling has shown an improved diurnal cycle of precipitation simulations (Clark et al., 2016; Woodhams et al., 2018), the atmospheric domain is set up in a domain of $3\text{ km} \times 3\text{ km}$ high resolution, with 350×350 grids points. The model domain covers the whole basin and is centred at the headwater area (Figure 1a). The vertical grid is a terrain-following grid of 40 levels up to a pressure top at 20 hPa. The adopted model physics are given in Table 1, with convection parameterization disabled, as employed in Zhang et al. (2019). In the WRF simulation, the unified Noah-LSM is used for the representation of water and energy exchanges at the land surface.

The Noah-LSM is widely used as the land component of climate and weather forecast models for simulating complex interactions between the land surface and the atmosphere (e.g., Davison et al., 2018; Erlandsen et al., 2017). It uses the diffusive form of Richards' equation and thermal diffusion equation for solving vertical

TABLE 1 Physical parameterizations for the WRF and WRF-Hydro simulation

Physics	Selected scheme
Microphysics	WRF single-Moment 6-class scheme (Hong & Lim, 2006)
Planetary boundary layer	Asymmetric Convective Model, version 2 (Pleim, 2007)
Cumulus parameterization	None
Longwave radiation	Rapid Radiative Transfer Model (Mlawer et al., 1997)
Shortwave radiation	Dudhia scheme (Dudhia, 1989)
Land surface	Noah-LSM (Chen & Dudhia, 2001)

water and heat transport in 2-m soil depth, with four-layer soil column of thickness 0.1, 0.3, 0.6, and 1.0 m from soil surface toward the bottom. The Noah-LSM calculates the latent heat flux using the diurnally dependent Penman potential evaporation-based approach (Chen et al., 1997; Mahrt & Ek, 1984), and it computes the sensible heat flux using the bulk heat transfer formulation based on Monin-Obukhov similarity theory (Chen & Dudhia, 2001). The ground heat flux is estimated following Fourier's law through the temperature gradient between surface temperature and soil temperature of the first layer.

2.3.2 | WRF-Hydro configuration

An extension package of multi-lateral hydrological processes is provided in WRF-Hydro, aiming at integrating atmospheric and hydrological prediction system (Gochis et al., 2015). In comparison to the Noah-LSM in the stand-alone WRF, WRF-Hydro additionally resolves the lateral movement of water in both surface and subsurface. The lateral routing processes in WRF-Hydro are resolved at a higher-resolution hydrological routing subgrid, which is composed of high-resolution terrain height, flow direction, channel network with Strahler stream order and basin grid. In this study, we prepare the hydrological routing subgrid at 300 m horizontal resolution based on the Hydrological data and maps based on Shuttle Elevation Derivatives at multiple Scales (HydroSHEDS) dataset. At each model timestep, infiltration excess and soil moisture content at four layers of Noah-LSM are disaggregated to this subgrid, then routed laterally.

The fundamental augmentations in WRF-Hydro include that (a) the infiltration excess is enabled to remain at the surface as ponded water, rather than being simply removed as in Noah-LSM in WRF, and (b) exfiltration is allowed to be generated from a fully saturated soil column caused by lateral flow. In this study, the saturated subsurface lateral flow is calculated using the method of Wigmosta et al. (1994) and Wigmosta and Lettenmaier (1999), as implemented in the Distributed Hydrology Soil Vegetation Model (DHSVM). It calculates the quasi-three-dimensional moisture transport which considers the effects of topography, saturated soil depth, and saturated hydraulic conductivity of different soil types. A fully unsteady, spatially explicit diffusive wave routing scheme (Julien et al., 1995; Ogden, 1997) based on the steepest descent (D8) method is used for overland flow routing. The overland flow which reaches the channel grid cells is taken as channel inflow, and the channel water is routed pixel-by-pixel using an explicit and 1-dimensional diffusive wave formulation (Gochis et al., 2015). The water drainage from the bottom soil is linked with an exponential bucketed model, which is used for estimating the contribution of baseflow discharge. Table 2 summarizes all the improved hydrological processes in the WRF-Hydro model. Above subsurface routing, overland flow routing, channel routing, and baseflow modelling are successively carried out in WRF-Hydro modelling. Once lateral routing processes have been completed, the ponded water depth and soil moisture content in the 300 m subgrid are linearly aggregated back to the 3-km WRF grid. Subsequently, the

TABLE 2 List of the description on the hydrological processes in WRF-Hydro

Physics processes	Description
Subsurface routing	Exfiltration from fully saturated soil columns contributes to infiltrations capacity excesses (Wigmosta & Lettenmaier, 1999); Subsurface lateral flow is computed from saturated layer.
Overland flow routing	Overland flow is subjected when ponded water exceeds a retention depth; Overland flow is lateral calculated with a fully unsteady, 2-D diffusive wave formulation (Julien et al., 1995; Ogden, 1997).
Channel routing	Overland flow the reaching channel grid is pixel-by-pixel routed with 1-D diffusive wave formulation; No overbank flow and no channel water losses (Gochis et al., 2015).
Baseflow	Drainage from bottom soil is calculated with an exponential function (Gochis et al., 2015).

spatially redistributed soil moisture feeds back to WRF atmospheric processes through the next iteration of Noah-LSM.

It is noted that the subsurface flow routing is restrained to a 2 m soil thickness, in accordance with the soil column described in Noah-LSM. The deep groundwater process is not resolved, the bucket baseflow model only aiming at conceptually representing the river baseflow. The channel flow routing is considered as a one-way coupled process in WRF-Hydro, so that channel inflow is received from the overland flow with no reversed retroaction. Therefore, only subsurface and overland flow routing are able to affect the atmospheric dynamics in the coupled WRF-Hydro framework (Fersch et al., 2020; Senatore et al., 2015).

The WRF-Hydro model allows being directly driven by specific atmospheric forcing in its "uncoupled mode" as a distributed hydrological model. Using observational input, the WRF-Hydro model can be optimized with hydrological parameters calibration processes (Yucel et al., 2015). We manually calibrated the relevant hydrological parameters in WRF-Hydro based on daily observed streamflow, which have been shown in Zhang et al. (2019). Further details on the WRF-Hydro model and its coupling system can be found in Gochis et al. (2015).

2.4 | Evaluation of model performance

To assess the model performance, we evaluate the WRF and coupled WRF-Hydro modelling results with the available observational dataset described in Section 2.2 at monthly, daily and sub-daily (3-hourly and hourly) temporal scale. The ability of the simulations in reproducing realistic surface meteorological conditions is assessed by comparing with CMFD and station data. The root-mean-square error (RMSE), mean bias deviation (MBD), Nash-Sutcliffe efficiency (NSE), and the Pearson correlation (r) are used as the performance measures and are detailed in Appendix A. We validate our simulations results

comprehensively, addressing particularly biases in the atmospheric modelling and land surface modelling parts.

3 | RESULTS

In this section, the modelling results of surface meteorological variables, energy, and water fluxes are described. The analysis starts from a general evaluation of spatial and temporal variations of simulated precipitation and temperature, and continues with an evaluation of surface meteorological variables at a diurnal scale. Afterward, the simulated diurnal surface energy fluxes are validated against with ground measurements, then compared at the basin scale, and further characterized spatially.

3.1 | Evaluation of surface meteorological conditions

3.1.1 | Spatiotemporal variations of daily precipitation and temperature

WRF and WRF-Hydro simulated daily precipitation and air temperature for the year 2008 are compared with the CMFD reference as Time-Latitude Hovmöller diagram in Figures 2 and 3. The comparison results for the years 2009 and 2010 are similar to those for the year 2008 in terms of patterns and magnitudes, therefore they are not shown here. Table 3 gives the statistical measures of daily values between simulations and CMFD for 3 years. As the Heihe River basin is located at the fringe of the monsoon zone, precipitation intensively occurs during May to September as short-term events formed by orographic lifting and convection (Wang et al., 2018; Li et al., 2019; Liu et al., 2017). Spatially, a high precipitation band is situated in the

mountainous area below 39.5°N due to the mountain blocking effect (Wang et al., 2017). Both WRF and WRF-Hydro reasonably simulate the spatiotemporal variations of precipitation in comparison to CMFD (Figure 2), with a significant daily correlation above 0.77 ($p < 0.01$) and spatial correlation above 0.87 ($p < 0.01$) for the study area. As shown in Figure 3, the distinct dynamics of temperature are well simulated by both WRF and WRF-Hydro models. The simulated spatiotemporal patterns of temperature showing a clear gradient from southern high mountains to the northern flat low area are very similar to those in CMFD. Statistically, the daily mean temperature shows both high correlation value of 0.98 ($p < 0.01$) and NSE value of 0.95 with respect to CMFD, and the spatial correlation of mean temperature exceeds 0.97 ($p < 0.01$). The overall spatiotemporal variability of precipitation and temperature are well captured by both WRF and WRF-Hydro simulations. However, both models reproduce a slightly warm bias of temperature about $\sim 0.85^\circ\text{C}$ with respect to CMFD mean temperature of -3.92°C and wet bias of precipitation about ~ 0.6 mm/day with respect to CMFD mean precipitation of 1.33 mm/day, which will be further discussed in the next section.

3.1.2 | Diurnal cycle of surface meteorological conditions

Simulated surface meteorological variables are further evaluated against the observational dataset at the diurnal scale. The spatially averaged instantaneous values of 2 m air temperature, precipitation rate, specific humidity, and 10 m wind speed in the headwater area are compared with 3 hourly CMFD datasets. The calculated monthly correlation coefficients and the biases are shown in Figure 4.

The monthly correlation coefficients for 2 m air temperature all exceed 0.83 ($p < 0.01$) for both WRF and WRF-Hydro simulations. The biases of the simulated air temperature are mostly within $\pm 0.8^\circ\text{C}$ during

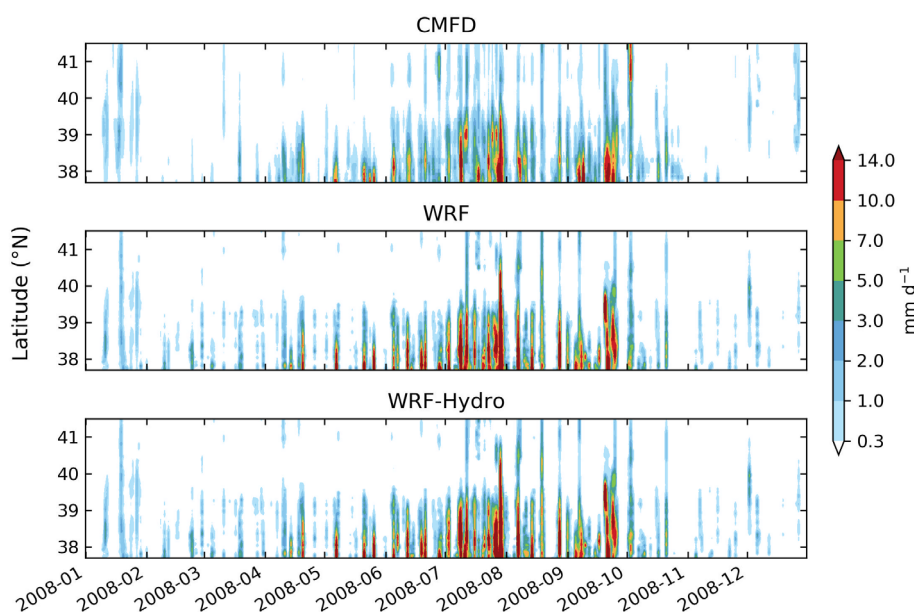


FIGURE 2 Time-Latitude Hovmöller diagrams displaying the daily precipitation in the year 2008 for CMFD, WRF and WRF-Hydro across the Heihe River basin

FIGURE 3 As in Figure 2, but for daily mean 2-m air temperature

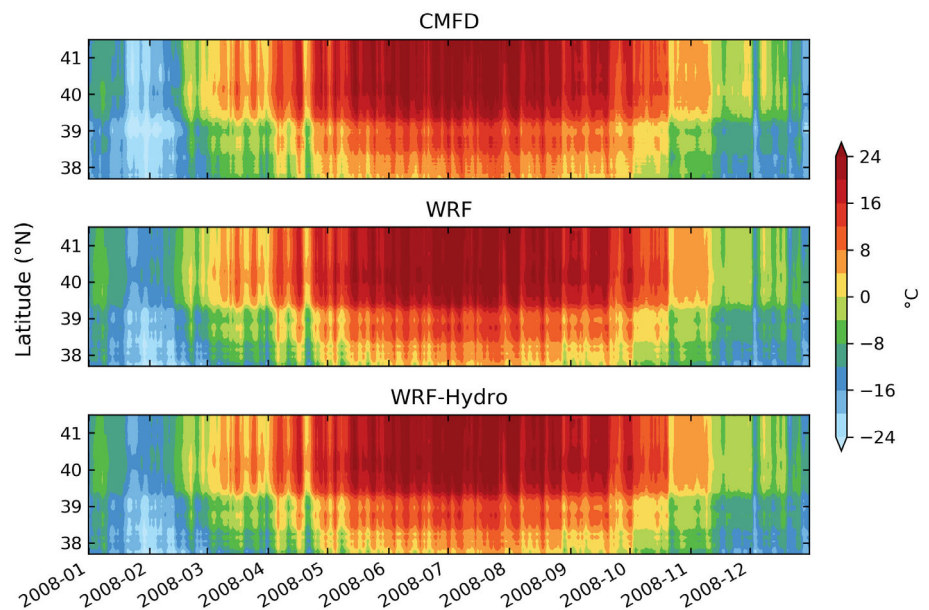


TABLE 3 Performance measures of RMSE, MBD, NSE and r between the simulated and observed daily precipitation (mm/d) and 2-m air temperature ($^{\circ}\text{C}$) spatially averaged for the headwater of Heihe River in the period 2008–2010

	WRF				WRF-Hydro			
	RMSE	MBD	NSE	r	RMSE	MBD	NSE	r
Precipitation	2.82	0.57	–	0.78	3.01	0.61	–	0.77
Temperature	2.05	0.90	0.95	0.98	2.12	0.82	0.95	0.98

the warm season (i.e., from March to October). However, a warm bias reaching $\sim 3.5^{\circ}\text{C}$ is observed in winter season when the average temperature is below -18°C (Figure 4a). Figure 5 further shows the monthly-averaged diurnal cycle of observed and simulated 2 m air temperature at two in-situ stations. At the Arou station with a higher altitude, both models well represent the diurnal variation of air temperature in the summer as well as the daytime temperature during the winter season (October to March). However, the night-time temperature in the winter is generally overestimated by the models, resulting in a smaller magnitude of diurnal variation in comparison to the observed data (Figure 5a). At the Guantan station, the simulated air temperature at the noontime is slightly higher than the observation (Figure 5b). Nevertheless, the scatter comparisons in Figure 6 and statistical measures in Table 4 show that both models well reproduce hourly air temperature in the summertime, with correlation coefficients of 0.91 ($p < 0.01$), NSE of 0.82, and mean bias $< 0.38^{\circ}\text{C}$. This confirms the small deviations to the observed records and small biases and high correlation compared to the gridded dataset (Figure 4a). It is worth noting that in terms of air temperature, WRF-Hydro shows slightly better performance (i.e., lower RMSE and mean bias values) than WRF at two ground stations.

For precipitation, the correlation coefficients are mostly between 0.1 and 0.6. Lower correlation coefficients are found in the dry season, whereas the mean biases are very small (Figure 4b). The low correlation values obtained for the dry season are mainly due to the fact that the models do not well represent the occurrence of some short-time and low precipitation events. In the summertime, the

overestimation of precipitation shows positive biases up to ~ 0.1 mm/h. Nevertheless, moderate correlation coefficients around 0.5 ($p < 0.01$) suggest that the diurnal precipitation variation is captured by WRF and WRF-Hydro approaches.

In Figure 4c, simulated specific humidity also shows a close correlation with the CMFD dataset. The calculated correlation coefficients are all above 0.7 ($p < 0.01$) and the mean percent biases range from -20% to $+10\%$.

The correlation of wind speed is mostly between 0.4 and 0.6, with no clear seasonal patterns. The monthly biases are exclusively positive, ranging from 0.5 m/s during the summertime to nearly 2 m/s in December and January (Figure 4d). This positive bias may be related to subgrid-scale orography conditions not well represented in the coarser CMFD dataset. The surface pressure, which is not shown in the figure, displays a correlation above 0.95 ($p < 0.01$) for all months.

The above results show that both WRF and WRF-Hydro simulations are able to represent the meteorological conditions in the study region, especially during the summertime. In the following sections, we focus on the simulated diurnal surface energy fluxes in the summer months.

3.2 | Diurnal cycle of surface energy fluxes at EC stations

The diurnal variations of simulated surface energy fluxes are firstly evaluated with flux tower measurements. Figures 7 and 8 show the

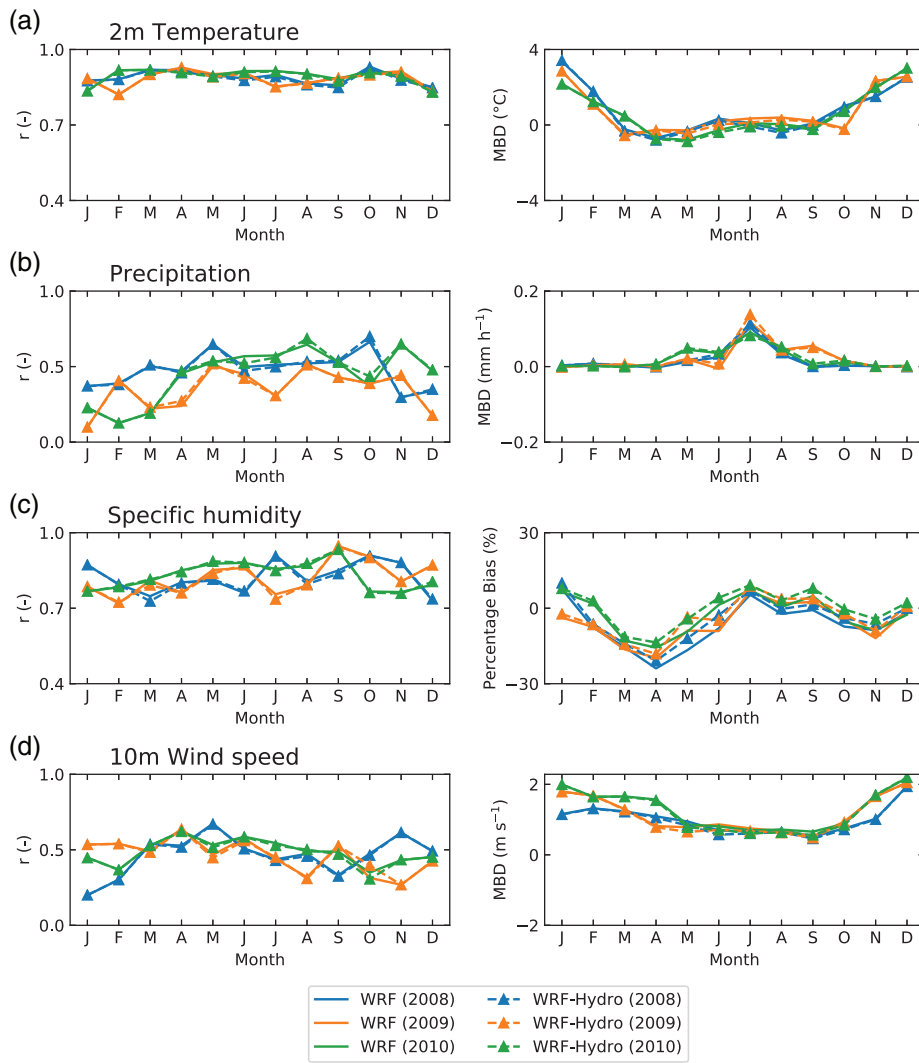


FIGURE 4 Monthly correlation and bias (WRF/WRF-Hydro versus CMFD) for the diurnal 3-h values for the period 2008–2010: (a) instantaneous 2-m air temperature, (b) precipitation rate, (c) instantaneous specific humidity and (d) instantaneous 10-m wind speed

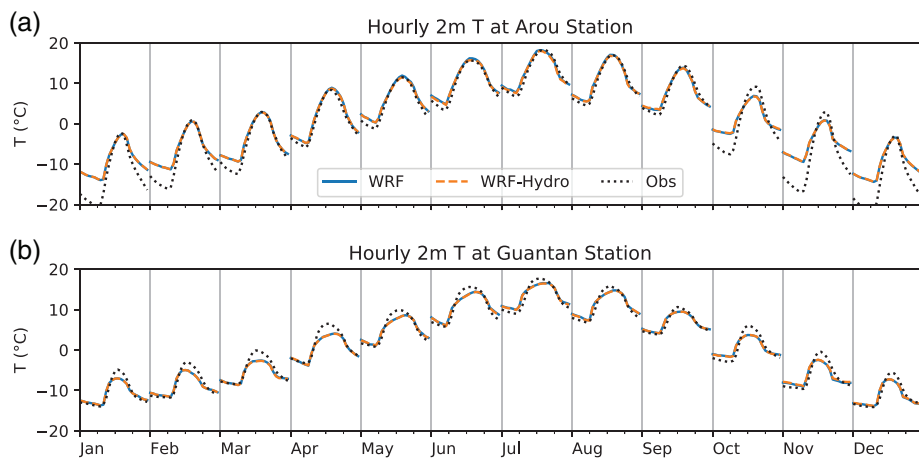


FIGURE 5 Monthly-averaged diurnal variation of 2-m air temperature from WRF, WRF-Hydro and station observation at (a) the Arou station and (b) the Guantan station for the period 2009–2010. The interval marks in x-axis of each month are 0, 6, 12 and 18 h of the local time

hourly comparison of measured and simulated net radiation (Rn), latent heat flux (LE), and sensible heat flux (H) at the Arou and Guantan EC stations, respectively. At the Arou station, time series comparisons indicate that the observed magnitudes of Rn and LE are well captured by the models, with Rn around 700 W/m² and LE up to

480 W/m², whereas the magnitude of H is overestimated (Figure 7). At the Guantan station, the models simulate a reasonable magnitude of LE and H, whereas Rn is underestimated during the noontime (Figure 8). Nevertheless, at both station sites, the occurrences of low Rn days caused by cloudy weather conditions are quite comparable

FIGURE 6 Scatter plot of hourly 2-m air temperature of WRF and WRF-Hydro versus observation at (a) the Arou station and (b) the Guantan station for the period June–September (JJAS) of 2009 and 2010

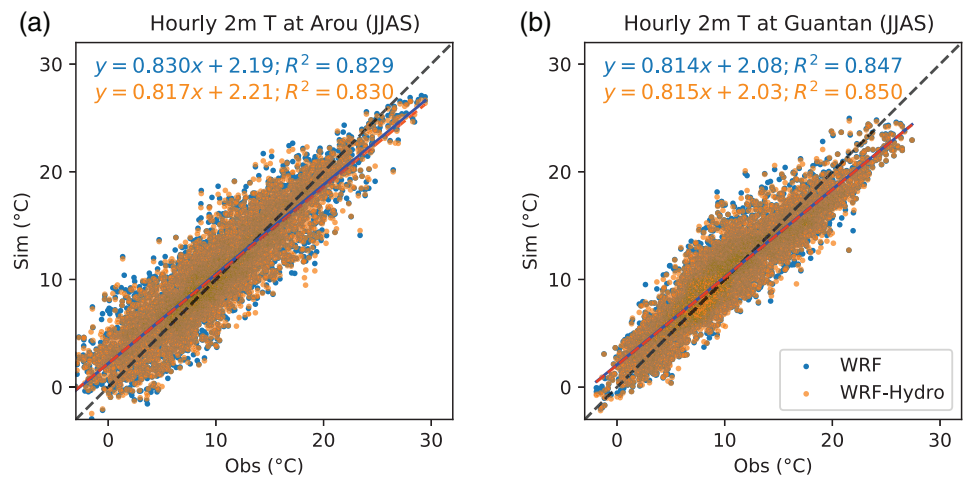


TABLE 4 Performance measures of RMSE, MBD, NSE and r between simulated and observed hourly 2-m air temperature ($^{\circ}\text{C}$) at the Arou and Guantan stations for June–September of 2009 and 2010

	WRF				WRF-Hydro			
	RMSE	MBD	NSE	r	RMSE	MBD	NSE	r
Arou station	2.24	0.38	0.82	0.91	2.21	0.27	0.83	0.91
Guantan station	1.88	0.15	0.84	0.92	1.86	0.10	0.84	0.92

between observations and simulations, which demonstrated that both WRF and WRF-Hydro well reproduce the inter-daily variations.

The mean diurnal cycles of surface energy fluxes split by month for two EC stations are shown in Figures 9 and 10. Table 5 lists the performance measures for simulations versus observations. In general, the diurnal patterns of surface energy fluxes are well captured in model simulations, showing comparable averaged values and SD, as well as the uniform increase and decrease tendencies related to solar rising and setting. Overall, the simulated R_n is slightly overestimated at the Arou station by 18 W/m^2 , whereas it is underestimated at the Guantan station by -31 W/m^2 . However, the simulated LE and H are generally higher than those observed at both station sites. The mean bias of peak value reaches 50 W/m^2 for LE and 70 W/m^2 for H at the Arou station, and up to 100 W/m^2 for both LE and H at the Guantan station. The averaged biases of simulated H and LE are around $15 \sim 20 \text{ W/m}^2$ and $13 \sim 17 \text{ W/m}^2$, respectively. Statistically, all the energy fluxes in comparison are associated with acceptable NSE values of $0.24 \sim 0.8$ and a high correlation above 0.77 ($p < 0.01$), indicating both models realistic represent the diurnal variations of surface energy fluxes.

The diurnal values of the Bowen ratio (H/LE) during daytime are shown in Figures 9d and 10d. The diurnal Bowen ratio generally ranges from 0.3 to 0.8 at the Arou station and from 0.4 to 1.5 at the Guantan station, indicating the relatively sufficient water status in the underlying vegetation surface, which is consistent with previous energy partitioning studies at two station sites (Wang, et al., 2019; Zhu et al., 2014). Comparing to the observations, both simulations appear to systematically overestimate the turbulent fluxes, but adequately represent the energy partitioning, which may be related to accurate measurements in EC system, as will be discussed later.

3.3 | Diurnal cycle of surface energy fluxes at basin scale

The basin-averaged hourly precipitation, R_n , LE, H, and ground heat flux (G) in the headwater of Heihe River are compared as a function of the day of the year, for exploring the diurnal cycle features of the surface energy fluxes. As the diurnal features of surface energy fluxes show similar interannual variations during the simulation period 2008–2010, Figure 11 only displays the comparison results between WRF-Hydro and WRF from April to October of the year 2008, containing the onset and retreat period of the East Asian summer monsoon. The monthly averaged diurnal cycles of energy fluxes are additionally shown in Figure 12 for the summer months from June to September of 3 years.

According to Figure 11a, the simulated summer precipitation exhibits favourable occurrence in the late afternoon and early morning, with a minimum at noontime. It is consistent with the previously observed diurnal precipitation pattern in this area (Li et al., 2019; Liu et al., 2017). A clear shift of diurnal shape and the magnitude of the surface fluxes is shown at the end of May corresponding to the monsoon onset, with an observed increase of LE and a decrease of H (Figure 11c,d). As shown in Figure 12 for the rainy season, the nocturnal values of LE are close to 0, and values of H are around $-5 \sim -10 \text{ W/m}^2$ during the night, in relation to the negative net radiation and inversed temperature gradient between land surface and air. R_n increases dramatically during the day and peaks at noontime. Visibly, G takes a lead of the increase in the morning and reaches its peak earlier than R_n , LE, and H, then it decreases gradually to stable and negative values at night. On average, the turbulent fluxes show distinct differences among the months. The monthly peak values of

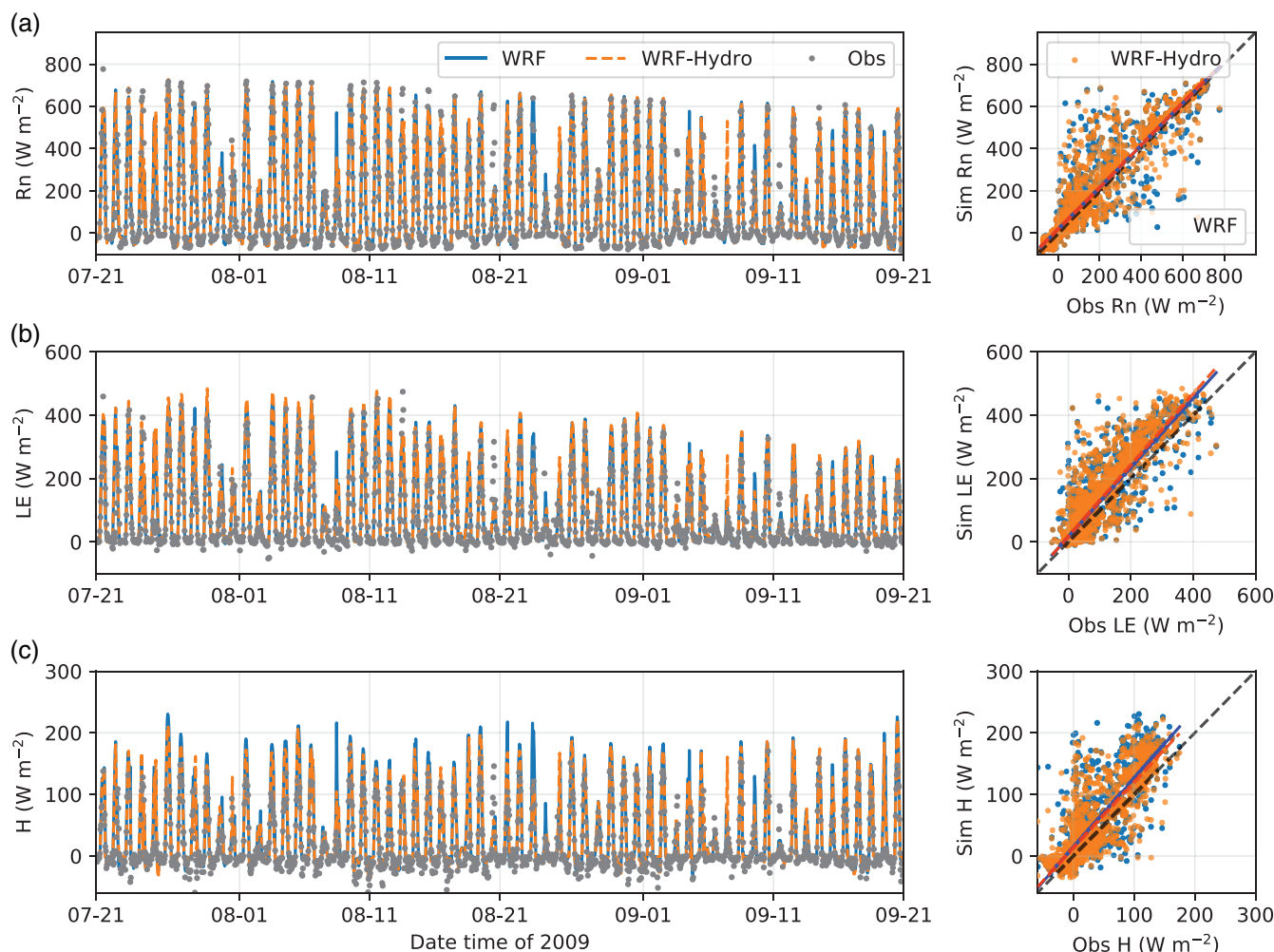


FIGURE 7 Hourly time series (left column) and scatter plot (right column) of simulated and observed (a) net radiation flux R_n , (b) latent heat flux LE , (c) sensible heat flux H at the Arou EC station in 2009

LE in July and August exceeding 200 W/m^2 , are generally higher than LE in June (Figure 12b), however, R_n and H show their highest values in June (Figure 12c,d). This change of the dominant turbulent fluxes suggests that LE in the study area is generally controlled by water-limited conditions rather than by radiation conditions, which is characteristic of the semi-arid region. From September on, both H and LE are decreased because of the reduction of available energy (Figure 11c,d). These features of energy fluxes are consistent with previous measurement analysis (Liu et al., 2011). Furthermore, the discontinuous spectra showing in the energy fluxes of LE and H are inherited from the diurnal cycle of R_n , which is modulated by the occurrence of precipitation events.

3.4 | Spatial signatures of diurnal surface energy fluxes

The spatial signatures of the diurnal cycle of surface energy fluxes are suitable for understanding the effect of topography, vegetation, and soil features captured in the coupled modelling (Xiang et al., 2017).

Since previous sections showed that lateral flow influences the regional water and turbulent fluxes, it is expected that the spatial variations of the diurnal energy fluxes are also impacted to some extent. Figure 13 presents the spatial pattern of the mean diurnal peak value and peak time of surface energy fluxes from June to September in 2008 for the headwater and its surrounding area. Comparing Figure 13 to Figure 1b, the peak value of R_n in high mountain peaks is relatively lower than it in the valley and the flat area, because of increased snow cover at higher elevation (Minder et al., 2016; Yu et al., 2017). The diurnal peak time of R_n shows slight spatial variations according to the terrain height, close to local noontime. The peak values of LE and H exhibit a close relationship with vegetation type (Figure 1c), with high values of LE in the vegetation-covered areas (e.g., grassland and cropland). In addition, LE in the southeastern part of the mountain is generally higher than it in the northwestern part due to the topographic enhancement of precipitation over higher areas (Pan et al., 2014; Yang et al., 2017; Zhang et al., 2019).

The spatial patterns of simulated LE are compared with the global and localized datasets in Appendix B. The highest LE occurs around the intermediate to higher elevation ecosystems in the headwater

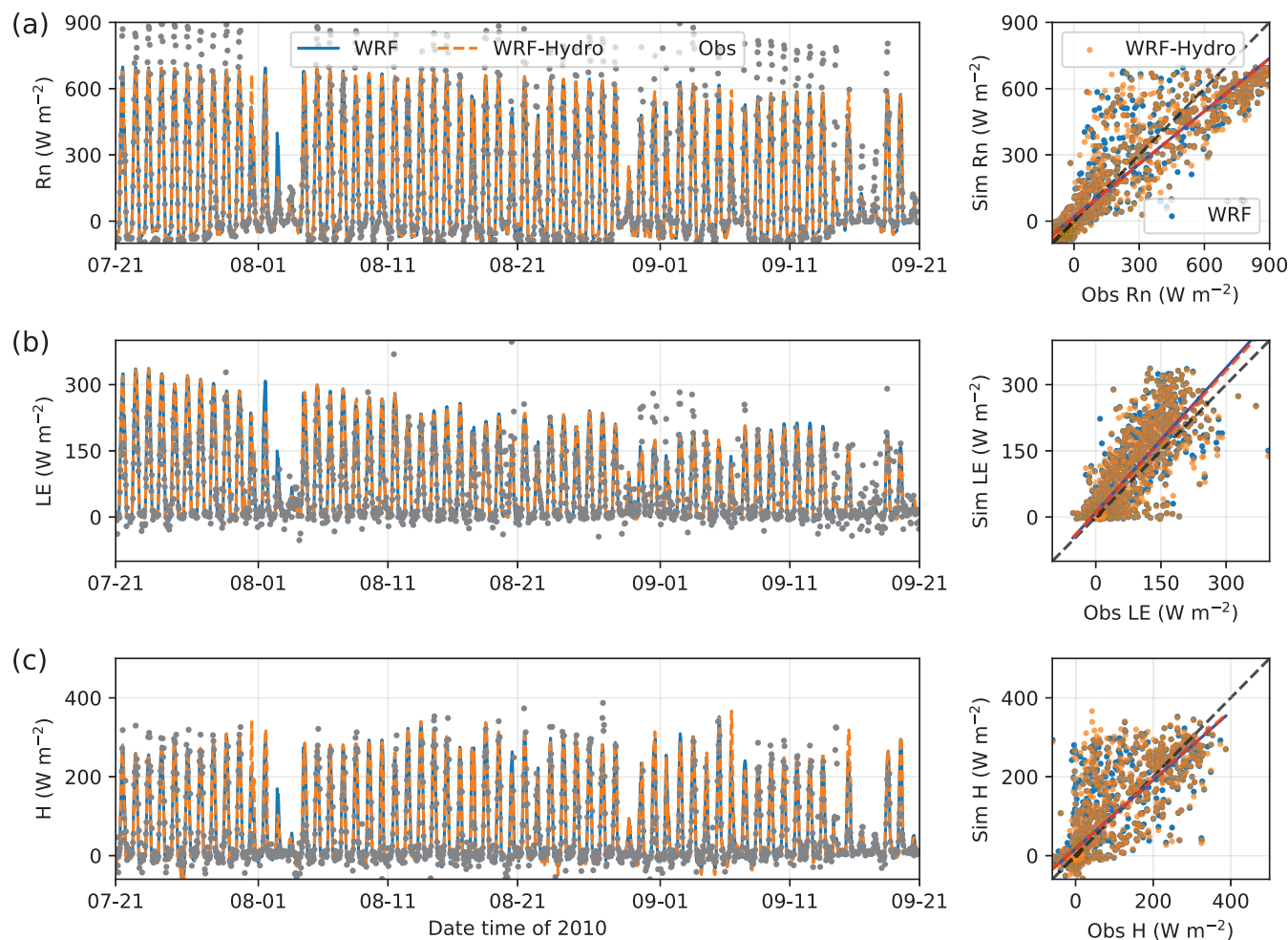


FIGURE 8 As in Figure 7, but for the Guantan EC station in 2010

area (shown in Figure B1), which is consistent with the previous finding of Gao et al. (2016). At the diurnal scale, the higher peak values of H are featured in the relatively flat terrain in the middle Heihe River basin and in the valley of the headwater area. The peak times of LE and H notably depend on the vegetation types, with a clear delay toward the afternoon in the barren area. The peak value of G shows high values at the barren area and low values at the vegetation-covered mountainous area, which is comparable with the spatial distribution of G estimated from multiple remote sensing data of Li et al. (2017). The peak time of G displays a distinct relation with topography, with an apparent delay at the mountain tops with respect to the flat area.

4 | DISCUSSION

4.1 | Uncertainties in model validations

The objectives of the study include the assessment of modelling results on reproducing surface meteorological fields and energy fluxes. As shown in Sections 3.1 and 3.2, the validation results confirm the

reasonable model performance but illustrate the consistent biases in comparison to the observational-based datasets. Such disparities can be partly identified as systematic biases, due to the fact that regional climate modelling is only driven by lateral boundary forcing. Many studies have indicated that the forcing data of lateral boundary largely affect the dynamic climate downscaling, in which the uncertainties in lateral boundary conditions remain in the simulated land surface dynamics (e.g., Massey et al., 2016; Moalafhi et al., 2017; Rocheta et al., 2017). In addition, the resolution mismatches in both point- and basin-scale assessment also necessarily produce systematic differences in the model validations (Bonekamp et al., 2018; Jousse et al., 2016). Nevertheless, despite the potential systematic biases, the effect of lateral flow processes can be investigated by intercomparing the simulation results between the coupled WRF-Hydro and WRF.

The biases shown in model validations also relate to the uncertainties in observational-based gridded datasets. The CMFD data merges observational records with various gridded data products, however, the observational stations are mostly situated in lowland and valleys, and only poorly distributed in high mountainous (He et al., 2020). With the orographic enhancement, larger uncertainties exist in the gridded dataset. This is particularly the case for the high-

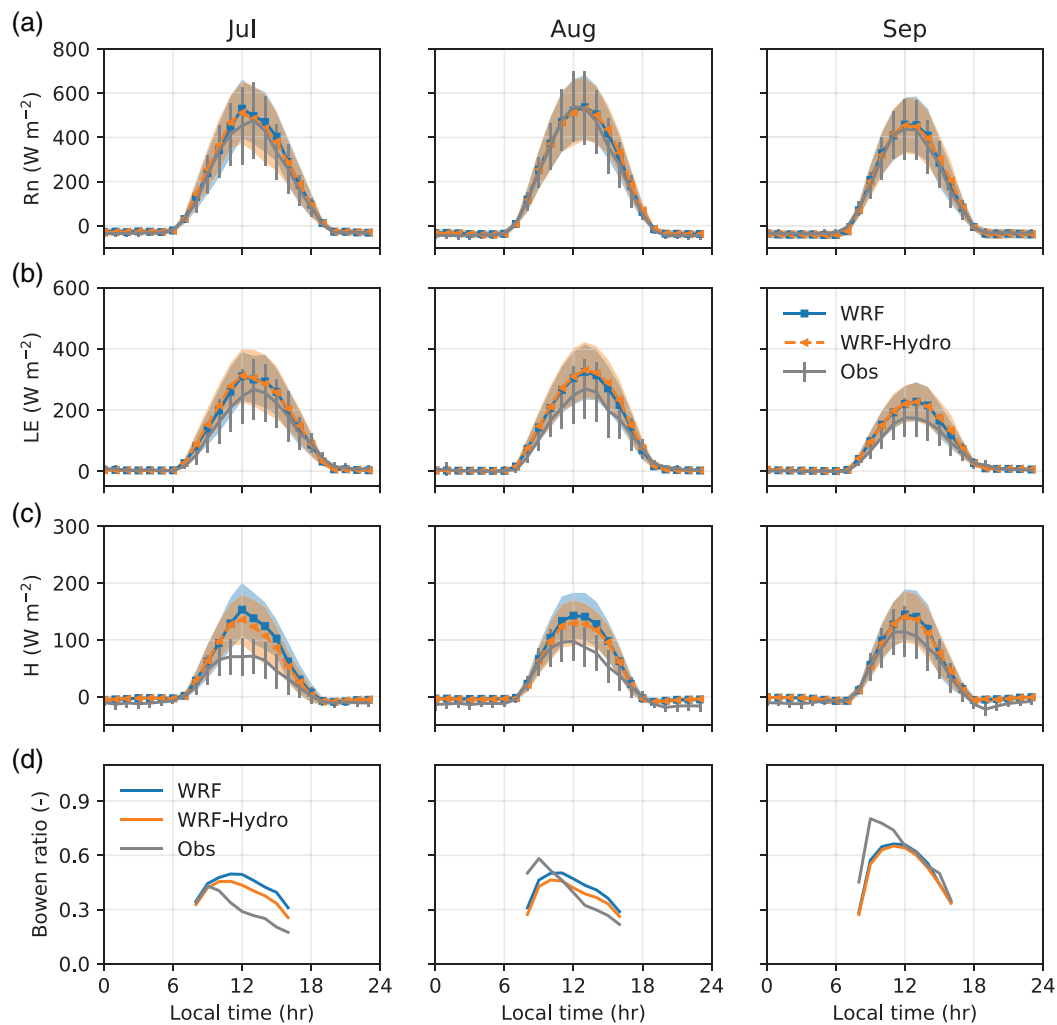


FIGURE 9 Monthly-averaged diurnal variations of simulated and observed (a) net radiation flux R_n , (b) latent heat flux LE , (c) sensible heat flux H and (d) Bowen ratio at the Arou EC station for the months July–September of 2009, with shading representing $\pm 75\%$ SD

alpine region with extremely complex topography, such as the study area. For example, the satellite-based product is merged in CMFD precipitation. However, Immerzeel et al. (2015) used an inverse approach with glacier mass balances to estimate the precipitation over an alpine catchment in Tibetan Plateau, and found that the high-altitude precipitation is more than twice as both station-interpolated and remote sensing-based precipitation products. Gao and Liu (2013) also concluded that satellite precipitation products generally underestimate moderate and heavy rainfall over the high mountains in Tibetan Plateau. For the near-surface temperature, Xie et al. (2017) found that CMFD data exhibits cold biases around -1.5°C on the Tibetan Plateau when observed temperatures are cold. The above-mentioned underestimation may counteract the biases of summer precipitation and winter temperature shown in Figure 4.

For the surface energy fluxes, the WRF and coupled WRF-Hydro simulations overestimate the turbulent fluxes LE and H at both Arou and Guantan sites. This disparity between simulation and observation is related to the uncertainties in EC measurements. The flux measurements in a single EC tower usually suffer from the

energy balance closure problem, with residuals imbalance around $10\% \sim 30\%$, and this lack of energy closure is more pronounced in half-hourly averaged values (Foken, 2008; Leuning et al., 2012). However, the energy balance in the model simulations is closed. Specific to the two EC towers at the Arou and Guantan stations, the residual imbalance in measured energy fluxes balance exceeds 16% and 25% in the summer months, respectively (Liu et al., 2011). Although diurnal energy residuals can be counterbalanced by energy storage in soil, vegetation and air, a part of imbalance is explicated by advective fluxes divergence, which generally suggests a possible underestimation of turbulent fluxes LE and/or H (Chakraborty et al., 2019; Liu et al., 2011; Ma et al., 2019; Twine et al., 2000). Additional uncertainties in the comparison may be noted when the measured turbulent fluxes are compared to 3 km model grid values, whereas the flux footprint of the Arou and Guantan EC towers are primarily representative of an area within a radius of 250 m (Liu et al., 2011). As a result, positive biases exhibit constantly in abundant studies when model simulated energy fluxes are compared to EC measurements (e.g., Aas et al., 2015; Chakraborty et al., 2019;

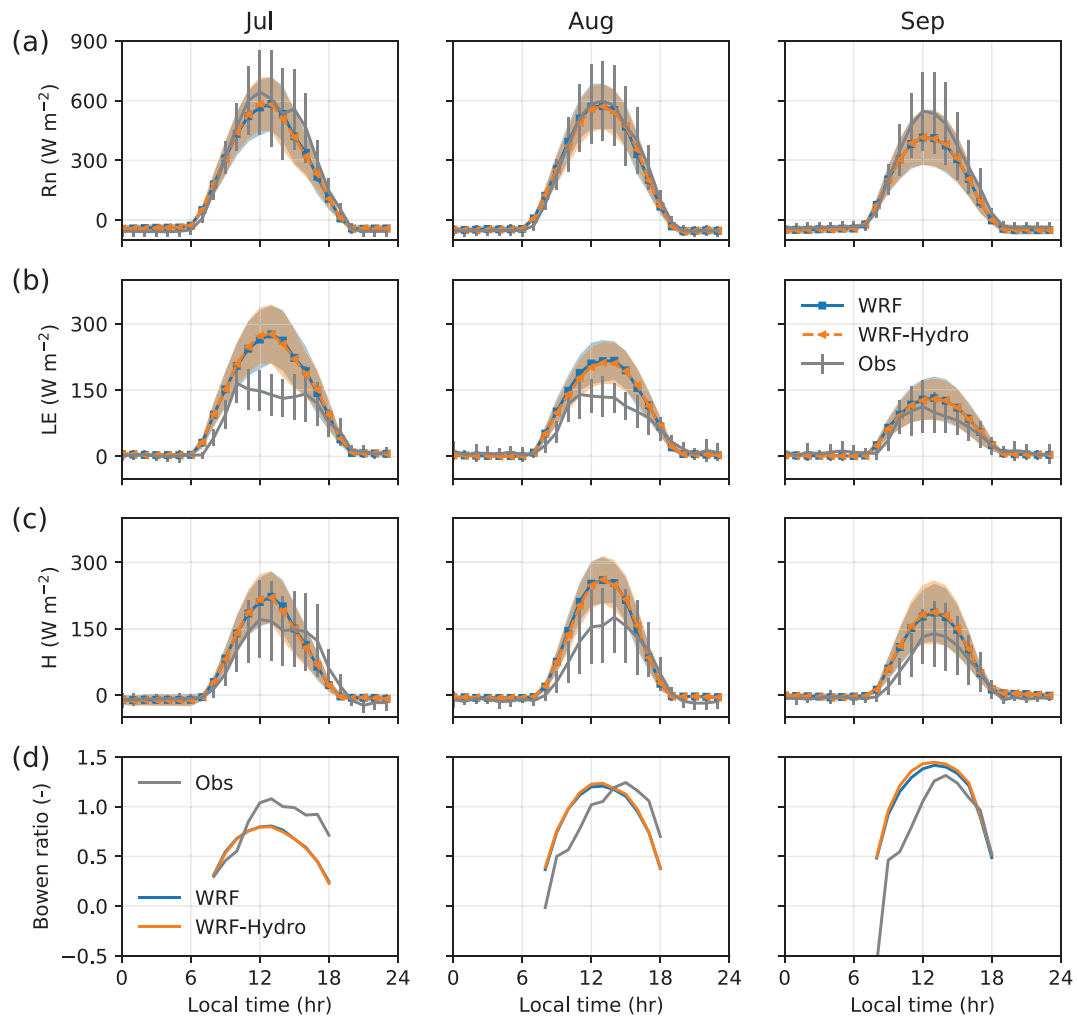


FIGURE 10 As in Figure 9, but for the Guantan EC station in 2010

TABLE 5 Performance measures of RMSE, MBD, NSE and *r* between simulated and observed hourly fluxes (W/m^2) of Rn, LE, H at Arou for July–September in 2009, and at Guantan for July–September in 2010

		WRF				WRF-Hydro			
		RMSE	MBD	NSE	<i>r</i>	RMSE	MBD	NSE	<i>r</i>
Arou station	Rn	93.8	18.0	0.80	0.91	91.7	18.2	0.80	0.91
	LE	62.7	20.4	0.61	0.87	65.1	22.8	0.58	0.88
	H	40.4	17.2	0.24	0.81	36.1	14.9	0.40	0.83
Guantan station	Rn	136.5	-31.2	0.80	0.91	136.4	-31.7	0.80	0.91
	LE	55.9	15.7	0.38	0.82	55.6	15.2	0.39	0.82
	H	64.8	13.6	0.53	0.77	65.4	13.5	0.54	0.77

Fersch et al., 2020; Ma et al., 2021; Lahmers et al., 2020; Xiang et al., 2017).

4.2 | Impact of the lateral flow in coupled modelling system

The comparison between WRF and fully coupled WRF-Hydro indicates the impact of lateral flow processes. For the meteorological

elements, both two models show a similar diurnal cycle and performance statistics. As shown in Figure 4, the correlation and bias values of air temperature and wind speed are quite close, indicating that the two models simulate very similar variations of temperature and wind elements. This is mainly related to the fact that the static dataset in both models is identical, which exhibits a similar surface roughness length for heat and momentum exchanges (Dong et al., 2018; Malhi, 1996). For the moisture variables, WRF-Hydro shows slightly higher correlation and bias in precipitation,

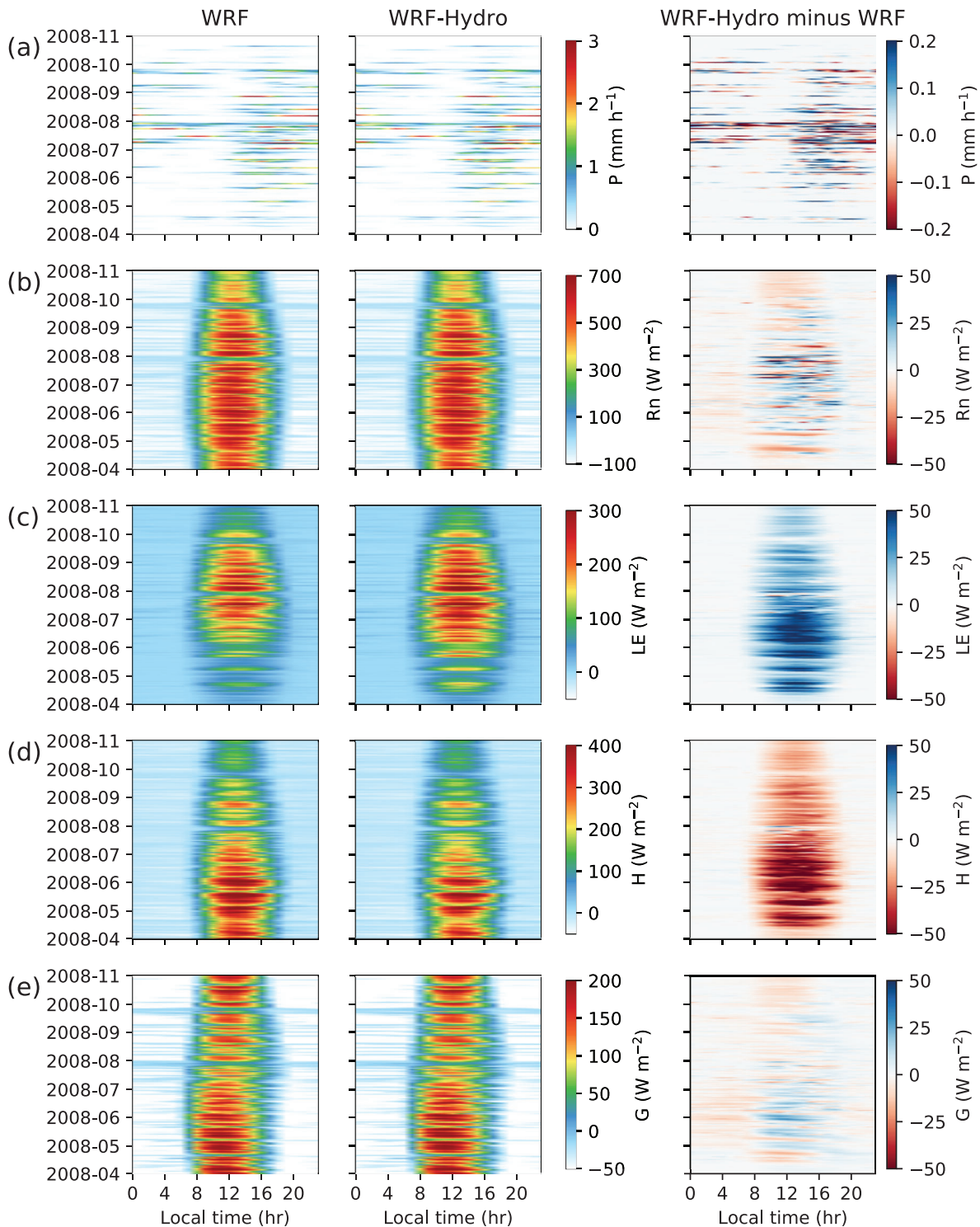
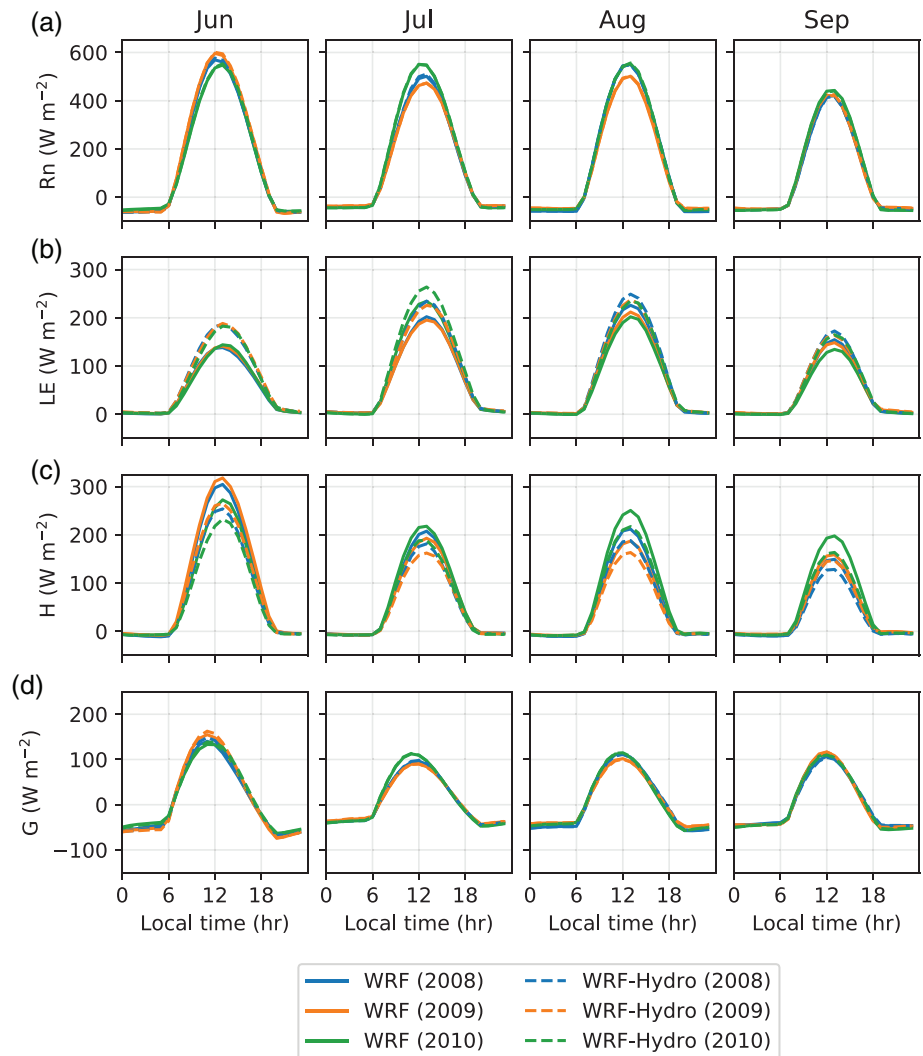


FIGURE 11 Hour of the day - day Hovmöller diagram displaying the diurnal cycle of (a) precipitation P , (b) net radiation flux R_n , (c) latent heat flux LE , (d) sensible heat flux H , and (e) ground heat flux G , spatially averaged for the headwater of Heihe River from WRF (left), WRF-Hydro (middle), and differences (WRF-Hydro minus WRF, right) for April–October in 2008

and slightly lower bias in specific humidity, suggesting that the diurnal variations of moisture fluxes are affected by the lateral flow. This more considerable impact of lateral flow on near-surface humidity than temperature is similar to that of Fersch et al. (2020).

Figures 7–10 show that the variations and mean values in surface energy fluxes and Bowen ratio between WRF and coupled WRF-Hydro are similar at two EC station locations. Slight differences in turbulent fluxes (LE and H) are identified at the Arou station, but statistically not significant. We further inter-compare the simulated top layer

FIGURE 12 Monthly-mean diurnal cycles of (a) net radiation flux R_n , (b) latent heat flux LE , (c) sensible heat flux H , and (d) ground heat flux G , spatially averaged for the headwater of Heihe River by WRF and WRF-Hydro for the months June–September in 2008–2010



soil water content with observations at two station sites (Figure 14). The simulated soil moisture variation at the Arou station is quite comparable with the observation. At the Guantan station, model results show a distinct increase in soil moisture at the beginning of August, which is associated with the fact that the precipitation is largely overestimated from July 27 to August 4, resulting in higher soil moisture until late September. Shown at both two station sites, it is found that the WRF and coupled WRF-Hydro simulated top layer soil moisture values are close, only with a slight difference within $0.03 \text{ m}^3/\text{m}^3$. Such slightly modified surface soil moisture does not evidently impact the turbulent fluxes at the station locations. This is attributed to the fact that both EC measurements are set up in a relatively flat area (Li et al., 2013; Liu et al., 2011). The hydro grid of 300-m represents a low topography gradient in these areas, so that the laterally routed overland and subsurface flow show a reduced influence in the land surface. A similar small impact on turbulent fluxes was also identified in Lahmers et al. (2020), who compared the coupled simulations with flux towers in grassland sites with a 250-m routing grid. As suggested by Ji et al. (2017) and Yang et al. (2021) in standalone land surface modelling, the influences of lateral flow are found more obvious when

LSM resolution is higher. Therefore, we expect a stronger impact on soil moisture and surface fluxes when the terrain routing subgrid is refined in a very fine grid-scale, for example, 100-m as applied in Fersch et al. (2020).

An appreciable impact of lateral flow on surface energy fluxes was shown at the basin scale. As shown in Figures 11 and 12, the diurnal cycles of R_n and G slightly differ between the two models, and such small differences still offer nearly the same amount of available energy ($R_n - G$) in their monthly averaged values. The diurnal differences in R_n are attributed to differences in the simulated weather conditions, as shown by the precipitation diurnal differences in Figure 11a. As suggested by Lahmers et al. (2020), lateral flow in WRF-Hydro might impact the location of convective precipitation at the diurnal scale. For the turbulent fluxes, LE in the daytime is notably higher in WRF-Hydro than that in WRF, and H is accordingly lower (Figure 11c,d), with a difference in their monthly-mean diurnal peak values around $50 \text{ W}/\text{m}^2$ in June and $20 \text{ W}/\text{m}^2$ in September (Figure 12b,c). As shown in Figure 13c,e, the differences in their diurnal peak values are mostly distributed at the locations where high topography gradients are featured (Figure 1b). These are closely

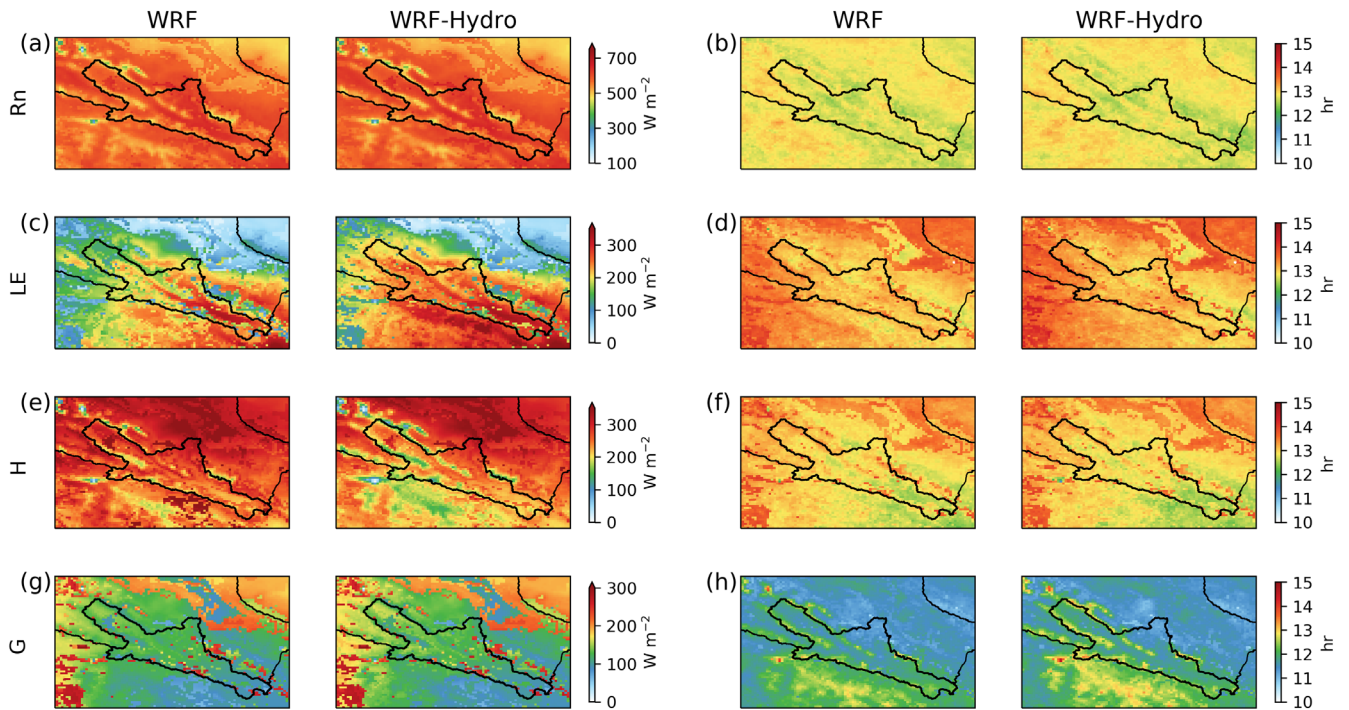


FIGURE 13 Spatial distribution of diurnal peak value (a, c, e, g) and peak time (b, d, f, h) of net radiation flux R_n (a, b), latent heat flux LE (c, d), sensible heat flux H (e, f) and ground heat flux G (g, h) for June–September in 2008

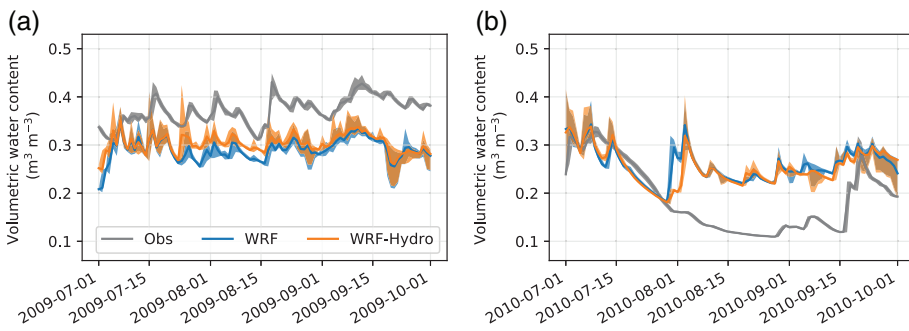


FIGURE 14 Daily variation of top soil layer volumetric water content at (a) the Arou station for July–September in 2009, and (b) the Guantan station for July–September in 2010. The shading represents the range of diurnal values, and line represents the daily mean values

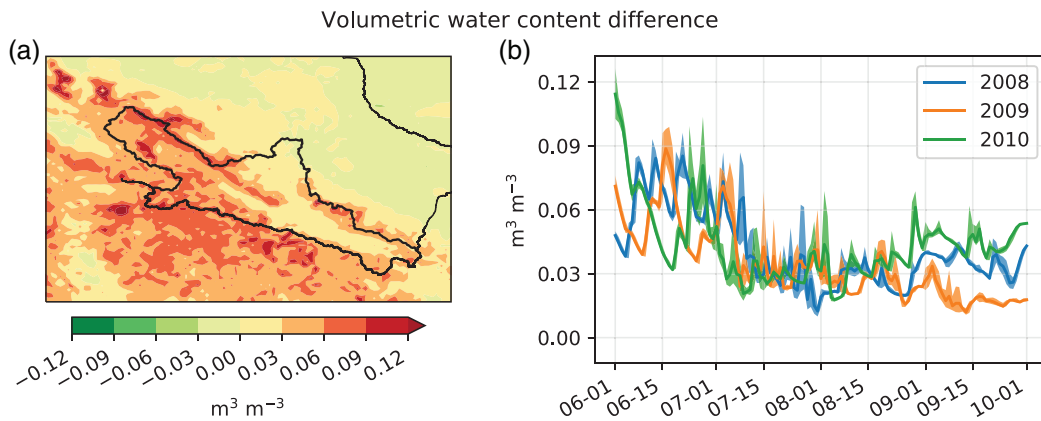


FIGURE 15 Difference (WRF-Hydro minus WRF) of top soil layer volumetric water content shown as (a) spatial distribution around the headwater of Heihe River, and (b) daily variation for the headwater of Heihe River for the months June to September in 2008–2010. The shading represents the range of diurnal values, and line represents the daily mean values

related to the differences in top layer soil moisture, as displayed in Figure 15. The WRF-Hydro simulated soil moisture is generally higher than the WRF simulated one, especially in the headwater area where the topography-driven spatial redistribution of soil moisture is largest (Figure 15a). The differences in basin-averaged soil moisture are around $0.09 \text{ m}^3/\text{m}^3$ during June, then decrease to $\sim 0.03 \text{ m}^3/\text{m}^3$ in September (Figure 15b), generally increase nearly 18%. This reveals that the lateral flow, mainly the routed overland flow, increases the memory of soil moisture in the coupled simulation (Arnault et al., 2019). Accordingly, the increase in soil moisture affects the diurnal energy flux partitioning, with an increased fraction of LE. Nevertheless, the peak times of areal averaged energy fluxes in the two simulations are almost unchanged.

The lateral flow affects the modelling system through the modification of soil moisture, and thus its impact depends on the strength of the coupling between soil moisture and the atmosphere. For example, the lateral flow was found to have a more pronounced enhancement of summer precipitation in West Africa than in Europe (Arnault et al., 2021), since West Africa is considered as a hot spot of soil moisture-atmosphere coupling (e.g., Koster et al., 2004). Being characterized by a semiarid-arid environment and high mountain terrain, our study area is not placed within the hot spots of land-atmosphere coupling (Koster et al., 2004), meanwhile, studies have shown that local precipitation is mainly modulated by remote atmospheric water transport (e.g., Wang, et al., 2018; Zhang et al., 2021). For this reason, representing lateral flow in the WRF model does not considerably change or degrade the model performance of simulated meteorological variables and energy fluxes at a diurnal scale over the study area. We have shown that lateral flow processes spatially increase (decrease) LE (H) over the hillslopes, however with no apparent impact on their diurnal peak time appearance (Figure 13c–f). The magnitude and spatial heterogeneity of surface energy fluxes are still consistent with the diverse vegetation ecosystems and the local terrain prescribed in the model (Figure 1), therefore, suggesting a realistic impact of lateral flow on diurnal surface energy fluxes.

4.3 | Limitations and perspectives

In the present study, the coupled WRF-Hydro model improves the realism of hydrological processes in regional climate models by allowing lateral water movement near the land surface. Even though the reliable surface energy fluxes are constrained by facticity of EC measurements and observation limitation, our results show that the coupled WRF-Hydro simulation very slightly and partly improves the simulated surface energy fluxes compared to the WRF atmospheric simulation. Nevertheless, we note that the groundwater lateral flow, which is not considered in this study, may functionally modulate the land surface variables via groundwater-surface water interactions, particularly over the low-lying areas where the groundwater table is shallow (e.g., Davison et al., 2018; Forrester & Maxwell, 2020; Maxwell et al., 2015; Sulis et al., 2017). While our model configuration approximates the hydrological processes across most of the high-

mountain terrain over this headwater area, further coupling physically-based groundwater schemes can improve the realistic representation of hydrological processes over the mountain valley and lower reaches in the desert (e.g., Wang et al., 2014; Xie et al., 2018). Moreover, coupling the addition of terrestrial hydrological schemes in model framework, such as irrigation scheme (e.g., Valmassoi et al., 2020), channel infiltration (e.g., Lahmers et al., 2019), and further two-way channel water-groundwater exchange (Fan et al., 2019), enables more realistic land-atmosphere feedbacks over the northern flat arid area.

Being driven by atmospheric lateral boundary only, the simulation of hydrometeorological variables in WRF-Hydro inherits the uncertainties and biases from atmospheric modelling. Using a model chain from bias-corrected high-resolution dynamical downscaling to terrestrial hydrological modelling, or jointly assimilating available observations in WRF-Hydro modelling can improve the simulation of surface energy flux (e.g., Abbaszadeh et al., 2020; Tsegaw et al., 2020). Additionally, the hydrological parameter optimization also restricts the coupled WRF-Hydro simulation, as the model calibration remains processed with adjusting conceptualized scaling factors of the most dominant parameters via offline simulations (Yucel et al., 2015; Zhang et al., 2019). Incorporating additional calibration tools (e.g., Silver et al., 2017; Wang, et al., 2019) and ingesting more physical parameters in LSM configuration (e.g., Zhang et al., 2020) for model calibration, as well as spatializing model parameters (Fersch et al., 2020; Rummler et al., 2019), may improve the representation of lateral hydrological processes in the coupled simulation. However, comprehensive calibration would require expensive computational demand, which is currently unrealistic for a longer-term (i.e., seasonal-to-annual) high-resolution coupled simulation. A trade-off between the hydrological parameter on model realism and computational availability has to be considered. In addition, the current parameterized lateral flow amounts including overland flow and subsurface flow fluxes are difficult to validate due to a lack of existing observation. With adequate computational resources along with reliable and extensive observations, the fully coupled modelling results can be further optimized by adapting model parameters with short-term simulations.

5 | SUMMARY AND CONCLUSIONS

In the pursuit of improving the terrestrial hydrological processes in regional climate modelling, this study aims at evaluating the performance of the fully coupled regional climate-hydrological modelling system in reproducing the diurnal surface energy fluxes, and ultimately assessing the impact of the lateral flow on the diurnal cycle of energy fluxes in an alpine catchment with complex terrain. Both WRF and coupled WRF-Hydro were found to have a reasonable performance in reproducing the precipitation and temperature in not only multi-temporal (daily-to-seasonal) but also varying spatial (point-to-regional) scales throughout the study area, the Heihe River basin. The diurnal variations of surface meteorological fields were overall well simulated by the models, albeit some biases depending on the season

were found. The simulated diurnal energy fluxes, as well as the hourly partitioning between sensible and latent heat flux, were comparable with EC tower observations during the summertime, indicating the equitable model ability in representing the magnitude and diurnal variation of the energy fluxes. The spatial patterns of diurnal surface energy fluxes were distinctly impacted by land heterogeneous surface, in relation to the diversity of vegetation ecosystems.

As a result of lateral flow, WRF-Hydro mostly increased the latent heat fluxes and reduced the sensible heat fluxes in their diurnal magnitude at a regional scale, although the net radiation and ground heat fluxes remained rarely changed. The impact on the diurnal peak time appearance of surface energy fluxes remained small. At the EC station points, the impact of lateral flow on the diurnal energy fluxes was rather concealed, which we attribute to the low topography gradient at the measurement sites. The results conceivably highlight the non-negligible role of lateral flow description on the surface energy fluxes where the topography is featured with complex and rugged terrain.

The results presented in this study are relevant for further researches which aim at investigating the land-atmosphere interactions employing a regional earth system model. The high resolution fully coupled modelling is successfully performed here even in extreme climate gradient, that is, tremendous elevation gradients and heterogeneous terrain. The benefits of the coupled model over the conventional regional weather and climate model, the enabled lateral flow and their atmospheric feedbacks, do not reduce the model skill of reproducibility. However, those further considered terrestrial hydrological processes improve the realism of earth system interactions, which is a step forwards in advancing Earth System modelling. This result encourages further investigations over regions to compass a wide range of climates and land covers using such a fully coupled atmospheric-hydrological modelling approach, which is of great importance to an improved understanding of land surface hydrological processes.

ACKNOWLEDGEMENTS

This work was financially supported by German Federal Ministry of Science and Education (BMBF) project SALDi (01LL1701B) and China Scholarship Council. Jöel Arnault and Jianhui Wei thank the funding support from German Science Foundation (DFG) grant AR 1183/2-1 and KU 2090/11-1, respectively. Ning Ma thanks the funding support from the National Natural Science Foundation (41801047). We would like to acknowledge Leibniz Supercomputing Center (LRZ) SuperMUC and the Computer cluster at KIT/IMK-IFU for providing resources for our calculations. We are grateful to the Editor and four anonymous reviewers for their helpful comments.

DATA AVAILABILITY STATEMENT

The China Meteorological Forcing dataset and the observational dataset used in this work are accessible online through registration at the National Tibetan Plateau Data Center (<https://doi.org/10.11888/AtmosphericPhysics.tpe.249369.file>) and the West Data Center of China (<http://card.westgis.ac.cn>), respectively. The soil texture data of Harmonized World Soil Database are available online at <http://www.fao.org/soils-portal/data-hub/soil-maps-and-databases/harmonized->

[world-soil-database-v12/en/](http://www.world-soil-database-v12/en/). The HydroSHEDS dataset are available online at <http://hydrosheds.cr.usgs.gov>. The data from the model simulations that support the findings of this study are stored in LRZ and available from the corresponding author upon request (zhenyu.zhang@kit.edu).

ORCID

Zhenyu Zhang  <https://orcid.org/0000-0002-9155-7378>

Joël Arnault  <https://orcid.org/0000-0001-8859-5173>

Patrick Laux  <https://orcid.org/0000-0002-8657-6152>

Ning Ma  <https://orcid.org/0000-0003-4580-0661>

Jianhui Wei  <https://orcid.org/0000-0001-8609-9600>

Harald Kunstmann  <https://orcid.org/0000-0001-9573-1743>

REFERENCES

- Aas, K. S., Berntsen, T. K., Boike, J., Eitzelmüller, B., Kristjánsson, J. E., Maturilli, M., Schuler, T. V., Stordal, F., & Westermann, S. (2015). A comparison between simulated and observed surface energy balance at the Svalbard Archipelago. *Journal of Applied Meteorology and Climatology*, 54, 1102–1119.
- Abbaszadeh, P., Gavahi, K., & Moradkhani, H. (2020). Multivariate remotely sensed and in-situ data assimilation for enhancing community WRF-Hydro model forecasting. *Advances in Water Resources*, 145, 103721.
- Arnault, J., Fersch, B., Rummeler, T., Zhang, Z., Quenum, G. M., Wei, J., Graf, M., Laux, P., & Kunstmann, H. (2021). Lateral terrestrial water flow contribution to summer precipitation at continental scale – A comparison between Europe and West Africa with WRF-Hydro-tag ensembles. *Hydrological Processes*, 4, 1–19.
- Arnault, J., Rummeler, T., Baur, F., Lerch, S., Wagner, S., Fersch, B., Zhang, Z., Kerandi, N., Keil, C., & Kunstmann, H. (2018). Precipitation sensitivity to the uncertainty of terrestrial water flow in WRF-Hydro: An ensemble analysis for central Europe. *Journal of Hydrometeorology*, 19, 1007–1025.
- Arnault, J., Wei, J., Rummeler, T., Fersch, B., Zhang, Z., Jung, G., Wagner, S., & Kunstmann, H. (2019). A joint soil-vegetation-atmospheric water tagging procedure with WRF-hydro: Implementation and application to the case of precipitation partitioning in the upper Danube River basin. *Water Resources Research*, 55, 6217–6243.
- Bonekamp, P. N. J., Collier, E., & Immerzeel, W. W. (2018). The impact of spatial resolution, land use, and spinup time on resolving spatial precipitation patterns in the Himalayas. *Journal of Hydrometeorology*, 19(10), 1565–1581.
- Chakraborty, T., Sarangi, C., Krishnan, M., Tripathi, S. N., Morrison, R., & Evans, J. (2019). Biases in model-simulated surface energy fluxes during the Indian monsoon onset period. *Boundary-Layer Meteorology*, 170, 323–348.
- Chen, F., & Dudhia, J. (2001). Coupling an advanced land surface-hydrology model with the Penn State-NCAR MM5 modeling system. Part I: Model implementation and sensitivity. *Monthly Weather Review*, 129, 569–585.
- Chen, F., Janjic, Z., & Mitchell, K. (1997). Impact of atmospheric surface-layer parameterizations in the new land-surface scheme of the NCEP mesoscale eta model. *Boundary-Layer Meteorology*, 85, 391–421.
- Chen, Y., Niu, J., Kang, S., & Zhang, X. (2018). Effects of irrigation on water and energy balances in the Heihe River basin using VIC model under different irrigation scenarios. *Science of the Total Environment*, 645, 1183–1193.
- Cheng, G., Li, X., Zhao, W., Xu, Z., Feng, Q., Xiao, S., & Xiao, H. (2014). Integrated study of the water-ecosystem-economy in the Heihe River basin. *National Science Review*, 1, 413–428.

- Chu, Q., Xu, Z., Peng, D., Yang, X., & Yang, G. (2015). Trends of surface humidity and temperature during 1951–2012 in Beijing, China. *Proceedings of the International Association of Hydrological Sciences*, 368, 126–131.
- Clark, P., Roberts, N., Lean, H., Ballard, S. P., & Charlton-Perez, C. (2016). Convection-permitting models: A step-change in rainfall forecasting. *Meteorological Applications*, 23, 165–181.
- Davison, J. H., Hwang, H. T., Sudicky, E. A., Mallia, D., & Lin, J. C. (2018). Full coupling between the atmosphere, surface, and subsurface for integrated hydrologic simulation. *Journal of Advances in Modeling Earth Systems*, 10, 43–53.
- Dong, H., Cao, S., Takemi, T., & Ge, Y. (2018). WRF simulation of surface wind in high latitudes. *Journal of Wind Engineering and Industrial Aerodynamics*, 179, 287–296.
- Dudhia, J. (1989). Numerical study of convection observed during the winter monsoon experiment using a mesoscale two-dimensional model. *Journal of the Atmospheric Sciences*, 46, 3077–3107.
- Dumedah, G., & Walker, J. P. (2014). Assessment of land surface model uncertainty: A crucial step towards the identification of model weaknesses. *Journal of Hydrology*, 519, 1474–1484.
- Erlandsen, H. B., Haddeland, I., Tallaksen, L. M., & Kristiansen, J. (2017). The sensitivity of the terrestrial surface energy and water balance estimates in the WRF model to lower surface boundary representations: A South Norway case study. *Journal of Hydrometeorology*, 18, 265–284.
- Fan, Y., Clark, M., Lawrence, D. M., Swenson, S., Band, L. E., Brantley, S. L., Brooks, P. D., Dietrich, W. E., Flores, A., Grant, G., Kirchner, J. W., Mackay, D. S., McDonnell, J. J., Milly, P. C. D., Sullivan, P. L., Tague, C., Ajami, H., Chaney, N., Hartmann, A., ... Yamazaki, D. (2019). Hillslope hydrology in global change research and earth system modeling. *Water Resources Research*, 55, 1737–1772.
- Fersch, B., Senatore, A., Adler, B., Arnault, J., Mauder, M., Schneider, K., Völsch, I., & Kunstmann, H. (2020). High-resolution fully coupled atmospheric-hydrological modeling: A cross-compartment regional water and energy cycle evaluation. *Hydrology and Earth System Sciences*, 24, 2457–2481.
- Foken, T. (2008). The energy balance closure problem: An overview. *Ecological Applications*, 18, 1351–1367.
- Forrester, M. M., & Maxwell, R. M. (2020). Impact of lateral groundwater flow and subsurface lower boundary conditions on atmospheric boundary layer development over complex terrain. *Journal of Hydrometeorology*, 21(6), 1133–1160.
- Gao, B., Qin, Y., Wang, Y., Yang, D., & Zheng, Y. (2016). Modeling eco-hydrological processes and spatial patterns in the upper Heihe basin in China. *Forests*, 7, 1–21.
- Gao, Y., Chen, F., Barlage, M., Liu, W., Cheng, G., Li, X., Yu, Y., Ran, Y., Li, H., Peng, H., & Ma, M. (2008). Enhancement of land surface information and its impact on atmospheric modeling in the Heihe River basin, Northwest China. *Journal of Geophysical Research*, 113, 90.
- Gao, Y., Li, K., Chen, F., Jiang, Y., & Lu, C. (2015). Assessing and improving Noah-MP land model simulations for the central Tibetan Plateau. *Journal of Geophysical Research: Atmospheres*, 120, 9258–9278.
- Gao, Y. C., & Liu, M. F. (2013). Evaluation of high-resolution satellite precipitation products using rain gauge observations over the Tibetan Plateau. *Hydrology and Earth System Science*, 17, 837–849.
- Gentine, P., Massmann, A., Lintner, B. R., Hamed Alemohammad, S., Fu, R., Green, J. K., Kennedy, D., & Vilà-Guerau de Arellano, J. (2019). Land-atmosphere interactions in the tropics - a review. *Hydrology and Earth System Sciences*, 23, 4171–4197.
- Gochis, D., Yu, W., Yates, D., 2015. The NCAR WRF-Hydro technical description and user's guide, version 3.0, NCAR Technical Document.
- Harding, K. J., & Snyder, P. K. (2012). Modeling the atmospheric response to irrigation in the Great Plains. Part I: General impacts on precipitation and the energy budget. *Journal of Hydrometeorology*, 13, 1667–1686.
- He, J., Yang, K., Tang, W., Lu, H., Qin, J., Chen, Y., & Li, X. (2020). The first high-resolution meteorological forcing dataset for land process studies over China. *Scientific Data*, 7, 25.
- Hong, S., & Lim, J. (2006). The WRF single-moment 6-class microphysics scheme (WSM6). *Journal of the Korean Meteorological Society*, 42, 129–151.
- Immerzeel, W. W., Wanders, N., Lutz, A. F., Shea, J. M., & Bierkens, M. F. P. (2015). Reconciling high-altitude precipitation in the upper Indus basin with glacier mass balances and runoff. *Hydrology and Earth System Sciences*, 19(11), 4673–4687.
- Ji, P., Yuan, X., & Liang, X.-Z. (2017). Do lateral flows matter for the hyper-resolution land surface modeling? *Journal of Geophysical Research: Atmospheres*, 122, 77–92.
- Jimenez, P. A., de Arellano, J. V.-G., Navarro, J., & Gonzalez-Rouco, J. F. (2014). Understanding land-atmosphere interactions across a range of spatial and temporal scales. *Bulletin of the American Meteorological Society*, 95, 14–17.
- Jousse, A., Hall, A., Sun, F., & Teixeira, J. (2016). Causes of WRF surface energy fluxes biases in a stratocumulus region. *Climate Dynamics*, 46, 571–584.
- Julien, P. Y., Saghafian, B., & Ogden, F. L. (1995). Raster-based hydrological modeling of spatially-varied surface runoff. *Journal of the American Water Resources Association*, 31, 523–536.
- Kerandi, N., Arnault, J., Laux, P., Wagner, S., Kitheka, J., & Kunstmann, H. (2018). Joint atmospheric-terrestrial water balances for East Africa: A WRF-hydro case study for the upper Tana River basin. *Theoretical and Applied Climatology*, 131, 1337–1355.
- Koster, R. D., Dirmeyer, P. A., Guo, Z., Bonan, G., Chan, E., Cox, P., Gordon, C. T., Kanae, S., Kowalczyk, E., Lawrence, D., Liu, P., Lu, C. H., Malyshev, S., McAvaney, B., Mitchell, K., Mocko, D., Oki, T., Oleson, K., Pitman, A., ... GLACE Team. (2004). Regions of strong coupling between soil moisture and precipitation. *Science*, 305(5687), 1138–1140.
- Lahmers, T. M., Castro, C. L., & Hazenberg, P. (2020). Effects of lateral flow on the convective environment in a coupled hydrometeorological modeling system in a semiarid environment. *Journal of Hydrometeorology*, 21, 615–642.
- Lahmers, T. M., Gupta, H., Castro, C. L., Gochis, D. J., Yates, D., Dugger, A., Goodrich, D., & Hazenberg, P. (2019). Enhancing the structure of the WRF-hydro hydrologic model for semiarid environments. *Journal of Hydrometeorology*, 20(4), 691–714.
- Leuning, R., Van Gorsel, E., Massman, W. J., & Isaac, P. R. (2012). Reflections on the surface energy imbalance problem. *Agricultural and Forest Meteorology*, 156, 65–74.
- Li, L., Li, J., Chen, H., & Yu, R. (2019). Diurnal variations of summer precipitation over the Qilian Mountains in Northwest China. *Journal of Meteorological Research*, 33, 18–30.
- Li, N., Jia, L., Lu, J., Menenti, M., & Zhou, J. (2017). Regional surface soil heat flux estimate from multiple remote sensing data in a temperate and semiarid basin. *Journal of Applied Remote Sensing*, 11, 016028.
- Li, X., Cheng, G., Ge, Y., Li, H., Han, F., Hu, X., Tian, W., Tian, Y., Pan, X., Nian, Y., Zhang, Y., Ran, Y., Zheng, Y., Gao, B., Yang, D., Zheng, C., Wang, X., Liu, S., & Cai, X. (2018). Hydrological cycle in the Heihe river basin and its implication for water resource management in endorheic basins. *Journal of Geophysical Research: Atmospheres*, 123, 890–914.
- Li, X., Cheng, G., Liu, S., Xiao, Q., Ma, M., Jin, R., Che, T., Liu, Q., Wang, W., Qi, Y., Wen, J., Li, H., Zhu, G., Guo, J., Ran, Y., Wang, S., Zhu, Z., Zhou, J., Hu, X., & Xu, Z. (2013). Heihe watershed allied telemetry experimental research (HiWater) scientific objectives and experimental design. *Bulletin of the American Meteorological Society*, 94, 1145–1160.
- Liu, S. M., Xu, Z. W., Wang, W. Z., Jia, Z. Z., Zhu, M. J., Bai, J., & Wang, J. M. (2011). A comparison of eddy-covariance and large aperture scintillometer measurements with respect to the energy balance closure problem. *Hydrology and Earth System Sciences*, 15, 1291–1306.
- Liu, X., Zhang, M., Wang, S., Wang, J., Zhao, P., & Zhou, P. (2017). Assessment of diurnal variation of summer precipitation over the Qilian

- Mountains based on an hourly merged dataset from 2008 to 2014. *Journal of Geographical Sciences*, 27, 326–336.
- Ma, N., Szilagyi, J., Zhang, Y., & Liu, W. (2019). Complementary-relationship-based modeling of terrestrial evapotranspiration across China during 1982–2012: Validations and spatiotemporal analyses. *Journal of Geophysical Research: Atmospheres*, 124, 4326–4351.
- Ma, N., Szilagyi, J., & Zhang, Y. (2021). Calibration-free complementary relationship estimates terrestrial evapotranspiration globally. *Water Resources Research*, 57(9). <https://doi.org/10.1029/2021wr029691>
- Mahrt, L., & Ek, M. (1984). The influence of atmospheric stability on potential evaporation. *Journal of Applied Meteorology and Climatology*, 23, 222–234.
- Malhi, Y. (1996). The behaviour of the roughness length for temperature over heterogeneous surfaces. *Quarterly Journal of the Royal Meteorological Society*, 122, 1095–1125.
- Massey, J. D., Steenburgh, W. J., Kniviel, J. C., & Cheng, W. Y. Y. (2016). Regional soil moisture biases and their influence on WRF model temperature forecasts over the intermountain west. *Weather and Forecasting*, 31, 197–216.
- Maxwell, R. M., Condon, L. E., & Kollet, S. J. (2015). A high-resolution simulation of groundwater and surface water over most of the continental US with the integrated hydrologic model ParFlow v3. *Geoscientific Model Development*, 8, 923–937.
- Meng, X., Lü, S., Zhang, T., Guo, J., Gao, Y., Bao, Y., Wen, L., Luo, S., & Liu, Y. (2009). Numerical simulations of the atmospheric and land conditions over the Jinta oasis in northwestern China with satellite-derived land surface parameters. *Journal of Geophysical Research*, 114, 6114.
- Minder, J. R., Letcher, T. W., & Skiles, S. M. (2016). An evaluation of high-resolution regional climate model simulations of snow cover and albedo over the Rocky Mountains, with implications for the simulated snow-albedo feedback. *Journal of Geophysical Research: Atmospheres*, 121, 9069–9088.
- Mlawer, E. J., Taubman, S. J., Brown, P. D., Iacono, M. J., & Clough, S. A. (1997). Radiative transfer for inhomogeneous atmospheres: RRTM, a validated correlated-k model for the longwave. *Journal of Geophysical Research*, 102, 663–682.
- Moalafhi, D. B., Sharma, A., Evans, J. P., Mehrotra, R., & Rocheta, E. (2017). Impact of bias-corrected reanalysis-derived lateral boundary conditions on WRF simulations. *Journal of Advances in Modeling Earth Systems*, 9, 1828–1846.
- Niu, G.-Y., Yang, Z.-L., Mitchell, K. E., Chen, F., Ek, M. B., Barlage, M., Kumar, A., Manning, K., Niyogi, D., Rosero, E., Tewari, M., & Xia, Y. (2011). The community Noah land surface model with multi parameterization options (Noah-MP): 1. Model description and evaluation with local-scale measurements. *Journal of Geophysical Research*, 116, 2109.
- Ogden, F. L. (1997). *CASC2D reference manual*. University of Connecticut.
- Orth, R., Dutra, E., & Pappenberger, F. (2016). Improving weather predictability by including land surface model parameter uncertainty. *Monthly Weather Review*, 144, 1551–1569.
- Pan, X., Li, X., Shi, X., Han, X., Luo, L., & Wang, L. (2012). Dynamic downscaling of near-surface air temperature at the basin scale using WRF—a case study in the Heihe River Basin, China. *Frontiers of Earth Science*, 6, 314–323.
- Pan, X., Li, X., Yang, K., He, J., Zhang, Y., & Han, X. (2014). Comparison of down-scaled precipitation data over a mountainous watershed: A case study in the Heihe River Basin. *Journal of Hydrometeorology*, 15, 1560–1574.
- Pleim, J. E. (2007). A combined local and nonlocal closure model for the atmospheric boundary layer. Part I: Model description and testing. *Journal of Applied Meteorology and Climatology*, 46, 1383–1395.
- Ran, Y. H., Li, X., Lu, L., & Li, Z. Y. (2012). Large-scale land cover mapping with the integration of multi-source information based on the Dempster-Shafer theory. *International Journal of Geographical Information Science*, 26, 169–191.
- Reichstein, M., Falge, E., Baldocchi, D., Papale, D., Aubinet, M., Berbigier, P., Bernhofer, C., Buchmann, N., Gilmanov, T., Granier, A., Grunwald, T., Havrankova, K., Ilvesniemi, H., Janous, D., Knohl, A., Laurila, T., Lohila, A., Loustau, D., Matteucci, G., ... Valentini, R. (2005). On the separation of net ecosystem exchange into assimilation and ecosystem respiration: Review and improved algorithm. *Global Change Biology*, 11, 1424–1439.
- Rocheta, E., Evans, J. P., & Sharma, A. (2017). Can bias correction of regional climate model lateral boundary conditions improve low-frequency rainfall variability? *Journal of Climate*, 30(24), 9785–9806.
- Rosero, E., Gulden, L. E., Yang, Z.-L., de Goncalves, L. G., Niu, G.-Y., & Kaheil, Y. H. (2011). Ensemble evaluation of hydrologically enhanced Noah-LSM: Partitioning of the water balance in high-resolution simulations over the little Washita River experimental watershed. *Journal of Hydrometeorology*, 12, 45–64.
- Rummler, T., Arnault, J., Gochis, D., & Kunstmann, H. (2019). Role of lateral terrestrial water flow on the regional water cycle in a complex terrain region: Investigation with a fully coupled model system. *Journal of Geophysical Research: Atmospheres*, 124, 507–529.
- Santanello, J. A., Dirmeyer, P. A., Ferguson, C. R., Findell, K. L., Tawfik, A. B., Berg, A., Ek, M., Gentile, P., Guillod, B. P., van Heerwaarden, C., Roundy, J., & Wulfmeyer, V. (2018). Land-atmosphere interactions: The LoCo perspective. *Bulletin of the American Meteorological Society*, 99, 1253–1272.
- Santanello, J. A., Peters-Lidard, C. D., Kumar, S. V., Alonge, C., & Tao, W.-K. (2009). A modeling and observational framework for diagnosing local land-atmosphere coupling on diurnal time scales. *Journal of Hydrometeorology*, 10, 577–599.
- Senatore, A., Mendicino, G., Gochis, D. J., Yu, W., Yates, D. N., & Kunstmann, H. (2015). Fully coupled atmosphere-hydrology simulations for the Central Mediterranean: Impact of enhanced hydrological parameterization for short and long time scales. *Journal of Advances in Modeling Earth Systems*, 7, 1693–1715.
- Shrestha, P., Sulis, M., Masbou, M., Kollet, S., & Simmer, C. (2014). A scale-consistent terrestrial systems modeling platform based on COSMO, CLM, and ParFlow. *Monthly Weather Review*, 142, 3466–3483.
- Silver, M., Karnieli, A., Ginat, H., Meiri, E., & Fredj, E. (2017). An innovative method for determining hydrological calibration parameters for the WRF-hydro model in arid regions. *Environmental Modelling and Software*, 91, 47–69.
- Skamarock, W.C., Klemp, J.B., Dudhia, J., Gill, D.O., Barker, D.M., Duda, M. G., Huang, X.Y., Wang, W., Powers, J.G., 2008. A description of the advanced research WRF version 3, NCAR technical note, National Center for Atmospheric Research, Boulder, Colorado
- Sulis, M., Williams, J. L., Shrestha, P., Diederich, M., Simmer, C., Kollet, S. J., & Maxwell, R. M. (2017). Coupling groundwater, vegetation, and atmospheric processes: A comparison of two integrated models. *Journal of Hydrometeorology*, 18, 1489–1511.
- Sun, X., Holmes, H. A., Osibanjo, O. O., Sun, Y., & Ivey, C. E. (2017). Evaluation of surface fluxes in the WRF model: Case study for farmland in rolling terrain. *Atmosphere*, 8, 1–23.
- Suni, T., Guenther, A., Hansson, H. C., Kulmala, M., Andreae, M. O., Arneth, A., Artaxo, P., Blyth, E., Brus, M., Ganzeveld, L., Kabat, P., de Noblet-Ducoudré, N., Reichstein, M., Reissell, A., Rosenfeld, D., & Seneviratne, S. (2015). The significance of land-atmosphere interactions in the earth system—iLEAPS achievements and perspectives. *Anthropocene*, 12, 69–84.
- Tsegaw, A. T., Pontoppidan, M., Kristvik, E., Alfredsen, K., & Muthanna, T. M. (2020). Hydrological impacts of climate change on small ungauged catchments – Results from a global climate model-regional climate model-hydrologic model chain. *Natural Hazards and Earth System Sciences*, 20, 2133–2155.
- Twine, T. E., Kustas, W. P., Norman, J. M., Cook, D. R., Houser, P. R., Meyers, T. P., Prueger, J. H., Starks, P. J., & Wesely, M. L. (2000). Correcting eddy-covariance flux underestimates over a grassland. *Agricultural and Forest Meteorology*, 103, 279–300.
- Valmassoi, A., Dudhia, J., Di Sabatino, S., & Pilla, F. (2020). Evaluation of three new surface irrigation parameterizations in the WRF-ARW

- v3.8.1 model: The Po Valley (Italy) case study. *Geoscientific Model Development*, 13, 3179–3201.
- Wagner, S., Fersch, B., Yuan, F., Yu, Z., & Kunstmann, H. (2016). Fully coupled atmospheric-hydrological modeling at regional and long-term scales: Development, application, and analysis of WRF-HMS. *Water Resources Research*, 52, 3187–3211.
- Wang, J., Wang, C., Rao, V., Orr, A., Yan, E., & Kotamarthi, R. (2019). A parallel workflow implementation for PEST version 13.6 in high-performance computing for WRF-hydro version 5.0: A case study over the midwestern United States. *Geoscientific Model Development*, 12, 3523–3539.
- Wang, L., Chen, R., Song, Y., Yang, Y., Liu, J., Han, C., & Liu, Z. (2018). Precipitation–altitude relationships on different timescales and at different precipitation magnitudes in the Qilian Mountains. *Theoretical and Applied Climatology*, 134, 875–884.
- Wang, P., Li, X., Tong, Y., Huang, Y., Yang, X., & Wu, X. (2019). Vegetation dynamics dominate the energy flux partitioning across typical ecosystem in the Heihe River basin: Observation with numerical modeling. *Journal of Geographical Sciences*, 29, 1565–1577.
- Wang, P., Yu, J., Pozdniakov, S. P., Grinevsky, S. O., & Liu, C. (2014). Shallow groundwater dynamics and its driving forces in extremely arid areas: A case study of the lower Heihe River in northwestern China. *Hydrological Processes*, 28, 1539–1553.
- Wang, X., Pang, G., Yang, M., Wan, G., & Liu, Z. (2018). Precipitation changes in the Qilian Mountains associated with the shifts of regional atmospheric water vapour during 1960–2014. *International Journal of Climatology*, 38, 4355–4368.
- Wang, Y., Yang, H., Yang, D., Qin, Y., Gao, B., & Cong, Z. (2017). Spatial interpolation of daily precipitation in a high mountainous watershed based on gauge observations and a regional climate model simulation. *Journal of Hydrometeorology*, 18, 845–862.
- Wehbe, Y., Temimi, M., Weston, M., Chaouch, N., Branch, O., Schwitalla, T., Wulfmeyer, V., Zhan, X., & Liu, J. (2019). Analysis of an extreme weather event in a hyper-arid region using WRF-hydro coupling, station, and satellite data. *Natural Hazards and Earth System Sciences*, 19, 1129–1149.
- Wigmosta, M. S., & Lettenmaier, D. P. (1999). A comparison of simplified methods for routing topographically driven subsurface flow. *Water Resources Research*, 35, 255–264.
- Wigmosta, M. S., Vail, L. W., & Lettenmaier, D. P. (1994). A distributed hydrology-vegetation model for complex terrain. *Water Resources Research*, 30, 1665–1679.
- Woodhams, B. J., Birch, C. E., Marsham, J. H., Bain, C. L., Roberts, N. M., & Boyd, D. F. A. (2018). What is the added value of a convection-permitting model for forecasting extreme rainfall over tropical East Africa? *Monthly Weather Review*, 146, 2757–2780.
- Xiang, T., Vivoni, E. R., Gochis, D. J., & Mascaro, G. (2017). On the diurnal cycle of surface energy fluxes in the north American monsoon region using the WRF-Hydro modeling system. *Journal of Geophysical Research: Atmospheres*, 122, 9024–9049.
- Xie, Z., Hu, Z., Gu, L., Sun, G., Du, Y., & Yan, X. (2017). Meteorological forcing datasets for blowing snow modeling on the Tibetan Plateau: Evaluation and intercomparison. *Journal of Hydrometeorology*, 18(10), 2761–2780.
- Xie, Z., Liu, S., Zeng, Y., Gao, J., Qin, P., Jia, B., Xie, J., Liu, B., Li, R., Wang, Y., & Wang, L. (2018). A high-resolution land model with groundwater lateral flow, water use, and soil freeze-thaw front dynamics and its applications in an endorheic basin. *Journal of Geophysical Research: Atmospheres*, 123, 7204–7222.
- Yang, B., Zhang, Y., & Qian, Y. (2012). Simulation of urban climate with high-resolution WRF model: A case study in Nanjing, China. *Asia-Pacific Journal of Atmospheric Sciences*, 48, 227–241.
- Yang, Y., Tang, J., Xiong, Z., & Dong, X. (2017). Evaluation of high-resolution gridded precipitation data in arid and semiarid regions: Heihe River basin, Northwest China. *Journal of Hydrometeorology*, 18, 3075–3101.
- Yang, Z., Huang, M., Berg, L., Qian, Y., Gustafson, W. I., Fang, Y., Liu, Y., Fast, J. D., Sakaguchi, K., & Tai, S. (2021). Impact of Lateral Flow on Surface Water and Energy Budgets Over the Southern Great Plains—A Modeling Study. *Journal of Geophysical Research: Atmospheres*, 126. <https://doi.org/10.1029/2020jd033659>
- Yu, L., Liu, T., Bu, K., Yang, J., Chang, L., & Zhang, S. (2017). Influence of snow cover changes on surface radiation and heat balance based on the WRF model. *Theoretical and Applied Climatology*, 130, 205–215.
- Yuan, X., Ji, P., Wang, L., Liang, X., Yang, K., Ye, A., Su, Z., & Wen, J. (2018). High-resolution land surface modeling of hydrological changes over the Sanjiangyuan region in the eastern Tibetan Plateau: 1. Model development and evaluation. *Journal of Advances in Modeling Earth Systems*, 10, 2806–2828.
- Yucel, I., Onen, A., Yilmaz, K. K., & Gochis, D. J. (2015). Calibration and evaluation of a flood forecasting system: Utility of numerical weather prediction model, data assimilation and satellite-based rainfall. *Journal of Hydrology*, 523, 49–66.
- Zhang, Z., Arnault, J., Laux, P., Ma, N., Wei, J., Shang, S., & Kunstmann, H. (2021). Convection-permitting fully coupled WRF-Hydro ensemble simulations in high mountain environment: impact of boundary layer- and lateral flow parameterizations on land-atmosphere interactions. *Climate Dynamics*. <https://doi.org/10.1007/s00382-021-06044-9>
- Zhang, Z., Arnault, J., Wagner, S., Laux, P., & Kunstmann, H. (2019). Impact of lateral terrestrial water flow on land-atmosphere interactions in the Heihe River basin in China: Fully coupled modeling and precipitation recycling analysis. *Journal of Geophysical Research: Atmospheres*, 124, 8401–8423.
- Zhang, A., Liu, W., Yin, Z., Fu, G., & Zheng, C. (2016). How will climate change affect the water availability in the Heihe River basin, Northwest China? *Journal of Hydrometeorology*, 17, 1517–1542.
- Zhang, J., Lin, P., Gao, S., & Fang, Z. (2020). Understanding the re-infiltration process to simulating streamflow in north Central Texas using the WRF-hydro modeling system. *Journal of Hydrology*, 587(4), 124902.
- Zhao, C., Piao, S., Huang, Y., Wang, X., Ciais, P., Huang, M., Zeng, Z., & Peng, S. (2016). Field warming experiments shed light on the wheat yield response to temperature in China. *Nature Communications*, 7, 530.
- Zheng, D., van der Velde, R., Su, Z., Wang, X., Wen, J., Booi, M. J., Hoekstra, A. Y., & Chen, Y. (2015). Augmentations to the Noah model physics for application to the Yellow River source area. Part II: Turbulent heat fluxes and soil heat transport. *Journal of Hydrometeorology*, 16, 2677–2694.
- Zhu, G., Lu, L., Su, Y., Wang, X., Cui, X., Ma, J., He, J., Zhang, K., & Li, C. (2014). Energy flux partitioning and evapotranspiration in a sub-alpine spruce forest ecosystem. *Hydrological Processes*, 28, 5093–5104.

SUPPORTING INFORMATION

Additional supporting information may be found in the online version of the article at the publisher's website.

How to cite this article: Zhang, Z., Arnault, J., Laux, P., Ma, N., Wei, J., & Kunstmann, H. (2021). Diurnal cycle of surface energy fluxes in high mountain terrain: High-resolution fully coupled atmosphere-hydrology modelling and impact of lateral flow. *Hydrological Processes*, 35(12), e14454. <https://doi.org/10.1002/hyp.14454>